

## Aim and Scope

The objective of the *Journal of Residuals Science & Technology* (JRS&T) is to provide a forum for technical research on the management and disposal of residuals from pollution control activities. The Journal publishes papers that examine the characteristics, effects, and management principles of various residuals from such sources as wastewater treatment, water treatment, air pollution control, hazardous waste treatment, solid waste, industrial waste treatment, and other pollution control activities. Papers on health and the environmental effects of residuals production, management, and disposal are also welcome.

## Editor-in-Chief

P. Brent Duncan  
*Department of Biology*  
*University of North Texas*  
*Denton, TX, USA*  
pduncan@unt.edu

## Editorial Advisory Board

Muhammad Abu-Orf  
*AECOM, USA*  
mohammad.abu-orf@aecom.com

Steve Dentel  
*University of Delaware, USA*  
dentel@udel.edu

Richard Dick  
*Cornell University, USA*  
rid1@cornell.edu

Guor-Cheng Fang, Ph.D.  
*Hungkuang University, Taiwan*  
gcfang@sunrise.hk.edu.tw

Robert Hale  
*Virginia Institute of Marine Science, USA*  
hale@vims.edu

Paul F. Hudak  
*University of North Texas, USA*  
hudak@unt.edu

Blanca Jimenez Cisneros  
*Inst. de Ingenieria, UNAM, Mexico*  
bjc@mumas.iingen.unam.mx

Julia Kopp  
*Technische Universitat*  
*Braunschweig, Germany*  
j.kopp@tu-bs.de

Uta Krogmann  
*Rutgers University, USA*  
krogmann@aesop.rutgers.edu

D. J. Lee  
*National Taiwan University, Taiwan*  
djlee@ntu.edu.tw

Giuseppe Mininni  
*Via Reno 1, Italy*  
mininni@irsa.rm.cnr.it

John Novak  
*Virginia Tech, USA*  
jtnov@vt.edu

Rod O'Connor  
*Chemical Consulting Services, USA*  
docroc34@hotmail.com

Nagaharu Okuno  
*The University of Shiga Prefecture,*  
*Japan*  
okuno@ses.usp.ac.jp

Jan Oleszkiewicz  
*University of Manitoba, Canada*  
oleszkie@ms.umanitoba.ca

Banu Örmeci  
*Carleton University, Canada*  
banu\_ormeci@carleton.ca

Ian L. Pepper  
*University of Arizona, USA*  
ipepper@ag.arizona.edu

Ioana G. Petrisor  
*Co-Editor-in-Chief*  
*Environmental Forensics Journal, USA*  
Environmental.Forensics@gmail.com

Bob Reimers  
*Tulane University, USA*  
rreimers@tulane.edu

Dilek Sanin  
*Middle East Technical University,*  
*Turkey*  
dsanin@metu.edu.tr

Mike Switzenbaum  
*Marquette University, USA*  
michael.switzenbaum@marquette.edu

Heidi Snyman  
*Golder Associates Africa (Pty) Ltd.,*  
*South Africa*  
hsnyman@golder.co.za

Ludovico Spinosa  
*Consultant at Commissariat*  
*for Env. Energ. in Region,*  
*Puglia, Italy*  
ludovico.spinosa@fastwebnet.it

P. Aarne Vesilind  
*Bucknell University, USA*  
aarne.vesilind@gmail.com


Doug Williams  
*California Polytechnic State*  
*University, USA*  
wmsenr@thegrid.net

**JOURNAL OF RESIDUALS SCIENCE & TECHNOLOGY**—Published quarterly—January, April, July and October by DEStech Publications, Inc., 439 North Duke Street, Lancaster, PA 17602.

Indexed by Chemical Abstracts Service. Indexed/abstracted in Science Citation Index Expanded. Abstracted in Current Contents/Engineering, Computing & Technology. Listed in ISI Master Journal.

Subscriptions: Annual \$219 per year. Single copy price \$60. Foreign subscriptions add \$45 per year for postage.

(ISSN 1544-8053)

 DEStech Publications, Inc.

439 North Duke Street, Lancaster, PA 17602-4967, U.S.A.

©Copyright by DEStech Publications, Inc. 2012—All Rights Reserved

---

# C O N T E N T S

---

## Research

**Quantification of Mineralogical and Amorphous Species in Chromium Ore Processing Residue** . . . . . 131

T. ALEXANDER BOECHER, JAMES M. TINJUM, PE, Ph.D. and XU, HUIFANG, Ph.D.

**Oil Removing Technology of Residues from Waste Oil-based Drilling Fluid Treated by Solid-liquid Separation** . . . . . 143

BING HOU, CHUAN LIANG, HAO DENG, SHUIXIANG XIE, MIAN CHEN and RONGSHA WANG

**Survival of *Ascaris* Ova in Desert Soils: A Risk Assessment** . . . . . 151

DAVID L. WILLIAMS, IAN L. PEPPER and CHARLES P. GERBA

**Removal of a Reactive Dye using Ash of Pulp and Paper Sludge** . . . . . 159

A. AZIZI, ALAVI MOGHADDAM and M. R. ARAMI



# Quantification of Mineralogical and Amorphous Species in Chromium Ore Processing Residue

T. ALEXANDER BOECHER<sup>1,\*</sup>, JAMES M. TINJUM, PE, Ph.D.<sup>2</sup> and XU, HUIFANG, Ph.D.<sup>3</sup>

<sup>1</sup>TRC Environmental Corporation, Grand Rapids, MI

<sup>2</sup>Engineering Professional Development, University of Wisconsin-Madison

<sup>3</sup>Geology and Geophysics, University of Wisconsin-Madison

**ABSTRACT:** Chemical and mineralogical quantification was performed on solid remains resulting from chromite ore processing (COPR) and for creating a material balance for better characterizing amorphous content (typically > 30% by weight). X-Ray diffraction, X-Ray fluorescence, and thermogravimetry were performed on unweathered and weathered COPR to quantify mineralogy, chemistry, amorphous content, and volatiles. Brownmillerite and several trace minerals found in unweathered COPR were converted to hydrated minerals including hydrotralcite, hydrogarnet, and CAC (chromium-bearing hydrocalumite) in weathered COPR. Aggregation of mineralogy, chemistry, sequestered volatiles, *in situ* pH, and Cr(VI) content of COPR permitted prediction of amorphous phases in COPR and likely sinks for Cr(VI).

## INTRODUCTION

**S**TUDY of the microstructure and chemical partitioning in complex industrial byproducts such as COPR is essential for tailored and effective management of potentially hazardous constituents. COPR is a byproduct of the processing of chromite ore process used for production of chromate salts [1] which are used in several industrial processes including tanning and electroplating [2]. Prior to 1976, hundreds of millions of kilograms of COPR were used as structural backfill in unlined and unregulated sites along the eastern seaboard of the United States. Since 1976, COPR has been classified as a hazardous waste by the EPA [3] and disposal has been governed by Resource Conservation and Recovery Act (RCRA) regulations [4]. Legacy sites, largely in New Jersey and Maryland, require continued attention. Two main issues have been at the forefront of COPR research: leaching of hexavalent chromium (Cr[VI]), a hazardous chemical [5,6,7], and expansion of COPR as a result of thermodynamic instability resulting from the mineralogy [8,9,10].

Historically, chromite ore ( $[\text{Mg,Fe}][\text{Cr,Al,Fe}]_2\text{O}_4$ ) was processed domestically using a process known as 'high-lime'. Soluble chromate salts are extracted from

chromite ore through a roasting process which promotes oxidation of mineralized trivalent chromium (Cr[III]) to aqueous Cr(VI). During the 'high-lime' process, crushed chromite ore is mixed with lime (CaO) and soda ash ( $\text{Na}_2\text{CO}_3$ ) and roasted at 1200°C [1,11]. This method is no longer used in the United States but has seen continued use in Russia, China, India, and Pakistan [11]. After extraction of soluble chromate salts via counter-current leaching sequences, residue is comprised of several high-density and thermodynamically unstable mineral phases known as "parent minerals" [1]. These minerals include brownmillerite ( $\text{Ca}_2[\text{Fe,Al}]_2\text{O}_5$ ), periclase (MgO), and excess lime (CaO) [4]. Under suitable pH, temperature, and moisture conditions COPR begins a complex series of reactions breaking down the predominant mineral, brownmillerite, into hydrogarnet and several other hydration products most of which are layered double hydroxides [12,13]. Growth of these brownmillerite hydration derivatives are influenced by original COPR composition, dissolved ions in pore fluid, pH, and depth relative to water table as well as other environmental variables [9,14,15,16]. The process of incorporating  $\text{CO}_2$  and  $\text{H}_2\text{O}$  into mineral structures and subsequent induration are referred to collectively as the weathering processes. As weathering progresses in COPR go there is a change in specific gravity ( $G_s$  3.09 to 2.81) as brownmillerite ( $G_s$  3.76) breaks down into hydrated products

\*Author to whom correspondence should be addressed.  
E-mail: ABoecher@tresolutions.com

( $G_s$  1.33, 2.10) [17]. A decrease in  $G_s$  corresponds to an increase in bulk volume if available porosity does not accommodate mineral expansion and as hydration progresses COPR can theoretically increase in volume by 10% or greater [8,9,14]. At least two studies have linked formation of ettringite, a sulfate-based mineral commonly found in cements, and calcium aluminum chromates (CACs) to swelling of COPR [9,14]. Macro-scale expansion causes millions of dollars of damage to underground utilities, asphalt caps, and building foundations at COPR fill sites worldwide [10].

Once COPR undergoes an appreciable amount of weathering lithification/cementation and mineralogy merit divide COPR into two categories granular grey-black (GB) and indurated hard-brown (HB) COPR [18]. GB COPR which is largely unchanged from the original byproduct is mineralogically composed of the high-temperature minerals brownmillerite and periclase, is granular, and has few hydrated minerals [4,10,19]. As weathering progresses, COPR indurates or hardens, turns a strong-brown or yellowish-brown color, and is designated HB COPR. HB COPR is strongly indurated containing an elevated Cr(VI) content [20] and has undergone significant mineralogical changes [4,8,9]. During this transformation process, amorphous or non-crystalline content rises dramatically in COPR. These phases cannot be detected by standard XRD quantification. Amorphous content exceeds 45% w/w in HB COPR alone. This segment of COPR chemistry has been largely ignored or marginalized in the literature but it may play a significant role in COPR expansion. Quantification of mineral and amorphous phases in COPR is an essential step for understanding how the material behaves *in situ* and for predicting future behavior and possible mitigation strategies.

COPR leaches Cr(VI) which may cause further complications especially at unlined fill sites. Rate of leaching depends on original concentrations, mineralogical uptake, pH, and several other environmental conditions [21]. Hexavalent chromium is a known carcinogen and exposure to human and biological communities via groundwater, surface water, and other pathways is of great concern [3,6]. Chromium metal occurs naturally in both hexavalent and trivalent forms [2]. Chromium is oxidized during industrial processing of chromite ore and leaches out as soluble chromate salts, and the process leaves unreacted chromite and remnant chromate [1,11,22]. Cr(III) is non-toxic and sparingly soluble because common chromium hydroxide compounds precipitate from solution which reduces leaching potential [22]. Cr(VI) adsorption to reductive soil

minerals such as goethite, kaolinite, montmorillonite, and free colloids of ferric iron is likely at low pH but adsorption is unfavorable at high pH conditions ( $\text{pH} > 11$ ) of COPR [22,23,24,25]. Chrysochoou *et al.* (2009) [26] found associations in COPR between amorphous iron compounds and Cr(VI) using several micro-analytical techniques. Trivalent concentrations are generally twice that of Cr(VI) in COPR [19] while total Cr content in COPR has been reported as high as 8% by weight and typically is 3–5% [19,27,21]. Chromite ore is processed for oxidizing naturally occurring Cr(III) into Cr(VI) because of its high solubility and subsequent extractability [1,11]. Cr(III) is sparingly soluble and does not readily oxidize in low pH soils (i.e.,  $\text{pH} < 5$ ) [2]. *In situ* Cr(III) is associated with minerals such as goethite or organic matter depending on soil pH [2,7,28]. Solubility and availability of Cr(VI) in COPR determines extent to which the metal is integrated into mineral structures.

Results are presented of quantification of mineral forms in COPR. These amorphous compounds make up between 30 and 50% of COPR by mass and mineralization of  $\text{CO}_2$  and  $\text{H}_2\text{O}$  supports identification of weathering-related minerals and amorphous compounds. Minerals connected with these weathering compounds may be associated with COPR expansion. Furthermore, characterization of amorphous content is presented with mass balance of COPR. Mass balance is instrumental for understanding availability of chromium and other elements in COPR and how they change with weathering. Mass balance is supported by multiple experimental techniques including quantitative X-Ray diffraction (XRD), X-Ray fluorescence (XRF), and thermogravimetry.

## MATERIALS

COPR was obtained from a fill site in Maryland, United States. Twelve samples were collected from the vadose zone (i.e., unsaturated and aerated zone above the water table) and identified as GB or HB based on color, specific gravity, and degree of cementation based on a classification system developed by Tinjum *et al.* [18]. GB COPR was classified (ASTM D2488) as a medium- to coarse-sized (i.e., 0.1 to 3 mm) sand with occasional hardened nodules (diameter = 0.5 cm). HB COPR was highly lithified with an observed coloring of 10YR 5/6 on the Munsell scale. Samples were sealed on-site to preserve *in situ* moisture conditions and to prevent contamination. During sample collection HB COPR was observed in thin layers occurring between

wider GB layers. HB layers were in the vadose zone above or at the water table allowing for more regular exposure to the atmosphere. Physical characterization of COPR included specific gravity (ASTM D854-06 Method B) [17], grain size distribution (ASTM D421) [17], and visual analysis. Average  $G_s$  for GB and HB were 3.091 and 2.806, respectively, which are within a standard range reported in the literature [18,29]. A GSD was not performed on HB COPR because induration has fused particles making this test irrelevant [18]. The pH of COPR is highly alkaline (pH > 11) for both GB and HB COPR [21].

## EXPERIMENTAL

### Bulk Chemical Analysis

COPR specimens were analyzed using XRF quantitative analysis under contract with ALS Chemex. The 'Whole Rock' analytical method was used and specimens were analyzed in duplicate. Five grams of each sample were prepared using 24 h air-dry desiccation followed by grinding of the material to < 75  $\mu\text{m}$ . Loss-On-Ignition (LOI) tests (ASTM D 7348-08) were performed as a part of the Whole Rock method. XRF tests were conducted on remaining material. A COPR sample (0.9 g) was added to 9.0 g of lithium borate flux (50/50  $\text{Li}_2\text{B}_4\text{O}_7 - \text{LiBO}_2$ ), mixed well, and fused in an auto fluxer at 1100°C. A flat molten glass disc was prepared from the resulting melt and analyzed by XRF spectrometry [30].

Oxidation state for each element was assumed to be the most common lowest state with the exception of  $\text{Fe}^{2+}$  and  $\text{Fe}^{3+}$ . A weight return of less than 100% indicates some trace elements were not detected.

### Mineral Phases

X-Ray diffraction analysis was performed on COPR to determine the most prevalent mineral structures. A standard specimen preparation method was designed for this experiment based on a recommended practice for COPR [4,18,31,32]. Specimens were placed in a desiccator for 24 h, hand-ground to pass a 75  $\mu\text{m}$  sieve, and mixed with 20% by weight corundum ( $\text{Al}_2\text{O}_3$ ) for quantitative analysis. X-ray diffraction analyses were carried out using a Scintag Pad V Diffractometer (Cu  $K\alpha$  radiation). The Scintag diffractometer was operated at 45 kV, 40 mA with Cu  $K\alpha$  radiation and used a 2 mm divergence slit, 4 mm incident scatter slit, 1 mm diffracted beam scatter slit, and 0.5 mm receiving slit.

Each sample was placed in a 2 mm deep square specimen well and scanned at 0.02° steps between 5° to 65° 2 $\theta$  with a 2 s dwell. Samples were scanned within 48 h desiccation to minimize crystal dehydration.

Quantitative XRD analysis was performed using a Rietveld Whole Pattern Fitting (WPF) function in Jade 9.0. Phase quantification of GB and HB COPR is complex and in some cases user-biased due to varying number of phases, amorphous content, and high iron content. Corundum was added as an internal standard for calculating the weight fraction of amorphous content and relative weights for each crystalline phase. Jade 9 uses relative intensity of peaks for an individual phase in reference to a corundum standard and experimentally determined relative intensity ratios (RIRs) for determining relative weight ratios. The International Center for Diffraction Data database (ICDD) was used for phase identification using Jade [33]. Table 1 displays mineralogical phases identified in COPR along with their respective PDF numbers and chemical formulae.

Thermogravimetric analysis (TGA) was performed by Edison Analytical Laboratories Inc. on a TGA2950 Thermogravimetric Analyzer (TA Instruments) [34]. A non-reactive atmosphere of nitrogen was used during the test to prevent any secondary reactions occurring with COPR specimens and thus adding mass. There is significant weight loss and as an example  $\text{Ca}(\text{OH})_2$  decomposes into CaO when normal ambient atmospheric air is used. If CaO is exposed to  $\text{CO}_2$  decomposition will be followed by a second reaction as CaO and  $\text{CO}_2$  react to form calcium carbonate [35]. The temperature program was a linear ramp from 30°C to 900°C at 10°C/min with data collection at 1 Hz. Specimens were held in platinum TGA pans. Mass spectra were taken every ten minutes during analysis with the purpose of identifying  $\text{H}_2\text{O}$  and  $\text{CO}_2$  off-gassing.

### Amorphous Content Analysis

A chemical profile of amorphous content in COPR was constructed by combining information from several different tests. XRF provides a breakdown of total elemental content in COPR by oxide weight while TGA provides liberation temperature and degree of crystallinity of low atomic number elements of the LOI. Quantitative XRD provides a breakdown of total elemental content held in crystalline form. Determining oxide content of amorphous content consisted of subtracting oxide weight determined via XRD from total oxide content of COPR determined by XRF. Sev-

**Table 1. Mineralogical Phases in COPR.**

Parent Minerals (i.e., minerals present in chromite ore roasting process)	PDF Number (ICDD) [33]	Chemical Formula
Brownmillerite	71-0667	(CaO) <sub>2</sub> (Fe,Al) <sub>2</sub> O <sub>3</sub>
Periclase	71-1176	MgO
Portlandite	44-1481	Ca(OH) <sub>2</sub>
Lime or quicklime (added)	37-1497	CaO
<b>Pure Hydration Products (from Brownmillerite)</b>		
Hydrogarnets	77-0240	(CaO) <sub>3</sub> Al <sub>2</sub> O <sub>3</sub> (H <sub>2</sub> O) <sub>6</sub>
Hydrotalcites	35-0965	(MgO) <sub>6</sub> (Al <sub>2</sub> O <sub>3</sub> )CO <sub>2</sub> •13.5H <sub>2</sub> O
Calcium Aluminum Chromium Oxide Hydrates (Cr-bearing hydrocalumite)	42-0063 48-0066	Ca <sub>4</sub> Al <sub>2</sub> O <sub>6</sub> (CrO <sub>4</sub> )•nH <sub>2</sub> O n = 9, 12, 14, 32
In addition, amorphous phases are present but not listed.		
<b>Other Hydration and Related Products (i.e., those containing Chromate, carbonate)</b>		
Brucite (hydration of periclase)	07-0239	Mg(OH) <sub>2</sub>
Portlandite (hydration of lime)	44-1481	Ca(OH) <sub>2</sub>
Calcite (by water/air infiltration)	05-0586	CaCO <sub>3</sub>
<b>Non-COPR Products</b>		
Quartz (e.g., sand in soil)	46-1045	SiO <sub>2</sub>

eral hypotheses were made as to the chemical structure of the amorphous content based on environmental conditions found in COPR including a pH > 11, standard temperature and pressure, and moderate levels of Cr(VI) in the leachate (50 ppm). TGA analysis was used to substantiate these hypotheses.

## RESULTS AND DISCUSSION

### Bulk Chemical Composition

Table 2 summarizes results from the quantitative XRF analysis. Major components were oxides of Ca, Fe, and Al which are typically found in COPR due to mineralogy of chromite ore and addition of CaO during processing [5,26]. Twelve samples were analyzed: 6 GB COPR and 6 HB COPR specimens. The most abundant metals in COPR are Ca, Fe, Al, Cr, and Mg. GB and HB COPR have similar concentrations of these main metals. However, HB COPR metals' concentrations may be diluted by additional CO<sub>2</sub> and H<sub>2</sub>O sequestered during induration. These same five metals have been discovered to be major constituents at many COPR sites [4,10,19]. When metal concentrations are corrected to account for difference in LOI, concentration difference between GB and HB is small (< 2%). Similarity between elemental chemistry of GB and HB COPR indicates no appreciable transfer of elements out of the COPR system through the weathering pro-

cess. Recrystallization or limited mass transfer via selective leaching may prevent material movement.

XRF mapping was performed on a sample of HB COPR (See Figure 1) using a scanning electron microscope in addition to bulk XRF analysis. The goal was to observe distribution of elements throughout COPR and qualitatively understand composition of observed interparticle crystal growth. The COPR particle was predominantly calcium and aluminum with nodules of

**Table 2. Bulk Chemistry from XRF Analysis (all data reported in wt.%).**

	GB		HB	
	Average	S.D.	Average	S.D.
SiO <sub>2</sub>	3.51	0.23	1.64	0.42
Al <sub>2</sub> O <sub>3</sub>	11.94	0.16	10.96	0.30
Fe <sub>2</sub> O <sub>3</sub>	21.28	0.21	17.91	0.88
CaO	36.85	0.70	29.35	0.88
MgO	8.29	0.24	6.13	0.29
Na <sub>2</sub> O	0.58	0.11	0.09	0.03
K <sub>2</sub> O	0.01	0.01	0.02	0.01
Cr <sub>2</sub> O <sub>3</sub>	2.85	0.65	2.84	1.04
TiO <sub>2</sub>	0.44	0.01	0.33	0.01
MnO	0.12	0.01	0.09	0.01
P <sub>2</sub> O <sub>5</sub>	0.01	0.01	0.01	0.00
SrO	0.01	0.00	0.01	0.00
BaO	0.01	0.00	0.01	0.00
CO <sub>2</sub> /H <sub>2</sub> O	12.42	0.87	28.93	1.64
<b>Totals</b>	<b>98.3</b>		<b>98.3</b>	

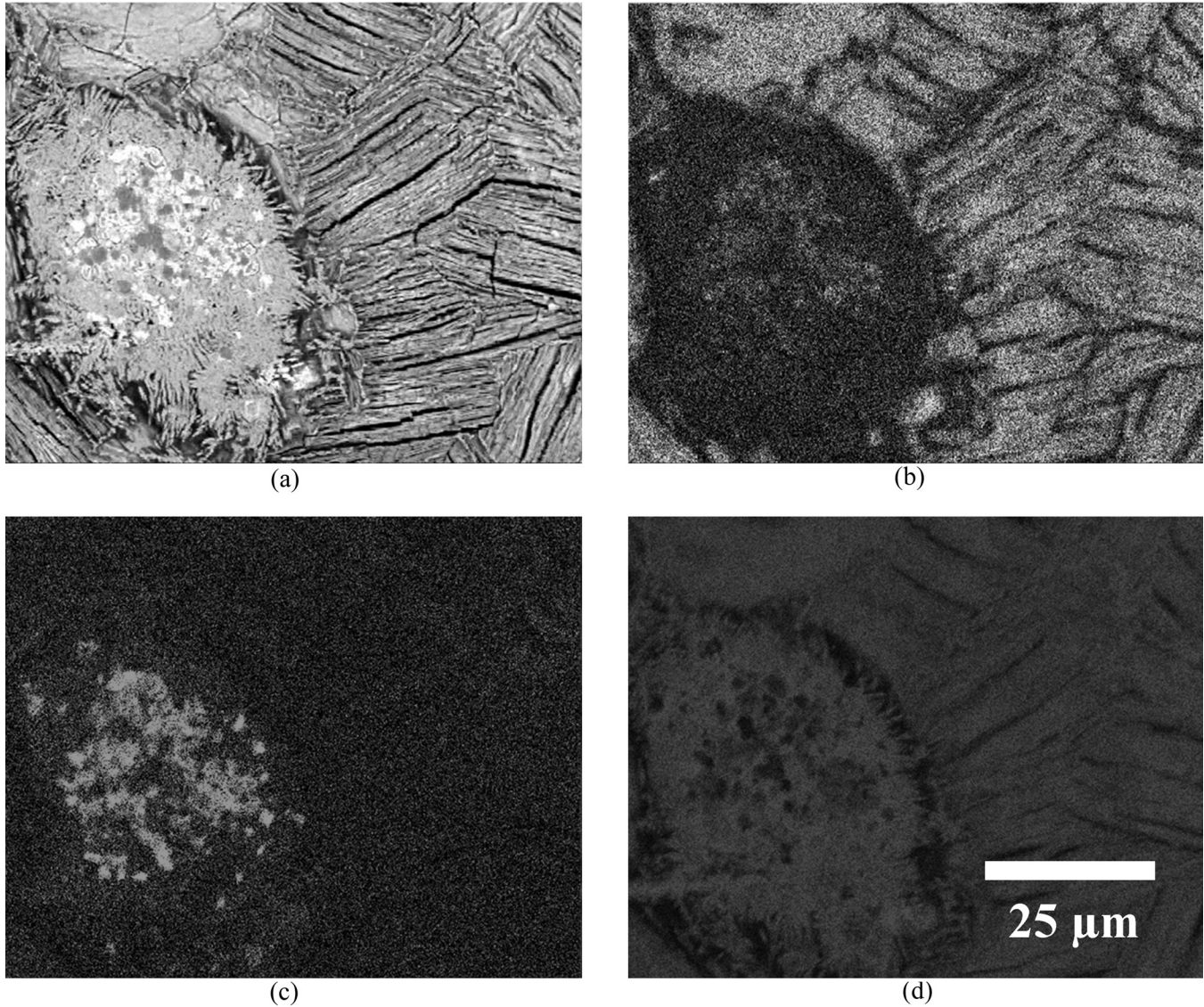


**Figure 1.** XRF map of HB COPR relic grain surrounded by hydrated mineral crystals. Base image (a) with overlays of (b) chromium, (c) iron, and (d) calcium. Overlays are not normalized.

iron and magnesium found near the core. While calcium and aluminum were found to migrate out of COPR particles as seen by calcium-aluminum-based interparticle mineral growth, iron and magnesium were found almost exclusively within the core of COPR particles. This observation suggests these minerals are calcium-aluminum-based hydrated minerals regularly observed in HB COPR.

Importance of these interparticle minerals to COPR remediation efforts is underscored by the observation that relatively chromium resides almost exclusively in new mineral growth. Hexavalent chromium has been previously observed migrating from COPR particles in layers of GB and concentrating in HB COPR layers [21]. High concentration of Cr(VI) within these miner-

als suggests an explanation for elevated Cr(VI) content in HB COPR relative to GB COPR.

### Mineral Phase Quantification

Table 3 reports quantitative results for 20 GB COPR and 10 HB COPR specimens from different sample buckets obtained from the study site. Over 40% w/w of GB COPR was brownmillerite. Hydrogarnet, hydroalcalite, and CAC were the most prevalent hydration products derived from brownmillerite which is consistent with the literature [4,20]. An XRD pattern of GB COPR is displayed in Figure 2. Ettringite has been reported at COPR sites [14] but was not found in any GB or HB COPR specimens in this study. Ettringite



**Table 3. Average Bulk Mineralogy from XRD Analysis (all data reported in wt.%).**

	RIR	GB (20 samples)		HB* (10 samples)	
		Average	S.D.	Average	S.D.
Brownmillerite	1.32	41.9	3.0	n.d.	0.0
Hydrogarnet	1.36	9.0	2.2	15.9	7.1
Portlandite	1.4	1.6	2.3	n.d.	0.0
Periclase	2.4	1.9	0.3	n.d.	0.0
Brucite	2.1	1.8	0.5	3.1	1.1
CAC·nH <sub>2</sub> O	2.0	6.1	1.7	12.4	9.2
Hydrotalcite	2.0	3.6	3.6	17.5	5.5
Calcite	2.0	1.9	1.0	3.5	1.1
Amorphous		30.5	2.8	46.3	16.1
<b>Totals</b>		<b>98.4</b>		<b>98.6</b>	

\*n.d. not detected

has also been reported as a common phase in COPR treated with sulfate-based reductants [6,14]. Although these XRF analyses did not determine sulfate concentrations, here COPR lacked sulfate (XRF weight percentage > 98%) needed to produce significant amounts of ettringite. Acid digestions further demonstrated that no appreciable sulfur was present to create ettringite

[21]. Therefore, it is unlikely that sulfate-based minerals such as ettringite are the cause of large-scale expansion at this COPR as postulated in previous literature [14] unless sulfur is injected as a remedial treatment.

Quantitative assessment for HB COPR provides a more difficult challenge due to the wide range of similarly structured hydration products and varying degrees of crystallinity [19,36]. An XRD pattern of HB COPR is provided in Figure 3. There were several hydration products detected in GB and HB COPR including CAC-9, CAC-12, CAC-14 as well as various Mg- and Al-based hydrotalcites. Calcium aluminum chromates were grouped under a single ‘CAC’ label for quantification since they have similar structure with a varying degree of hydration [4]. Overlapping peaks between 8° and 12° 2θ were identified by limiting ability of the quantification software to modify lattice constants and thus narrowly defining each peak width. These peaks were subsequently identified as CAC-9, CAC-12, and hydrotalcite.

Several techniques were attempted to increase accuracy of HB COPR quantification. One hypothesis was that hydrated minerals dehydrated during specimen preparation and handling interfered with accurate

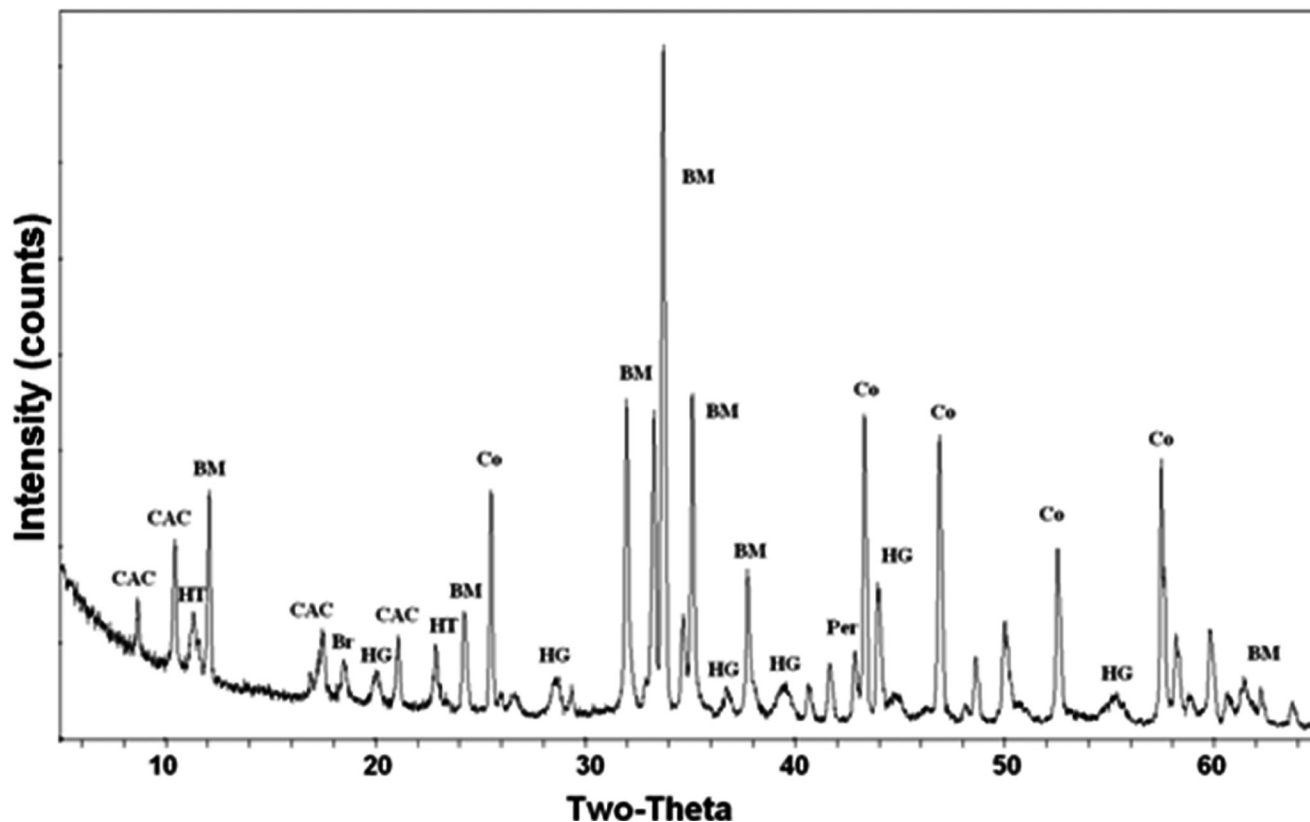


**Figure 2.** XRD pattern of GB COPR (BM: Brownmillerite; Per: Periclase; CAC: Calcium Aluminum Chromate 9 or 14; Br: Brucite; HG: Hydrogarnet; Co: Corundum standard).

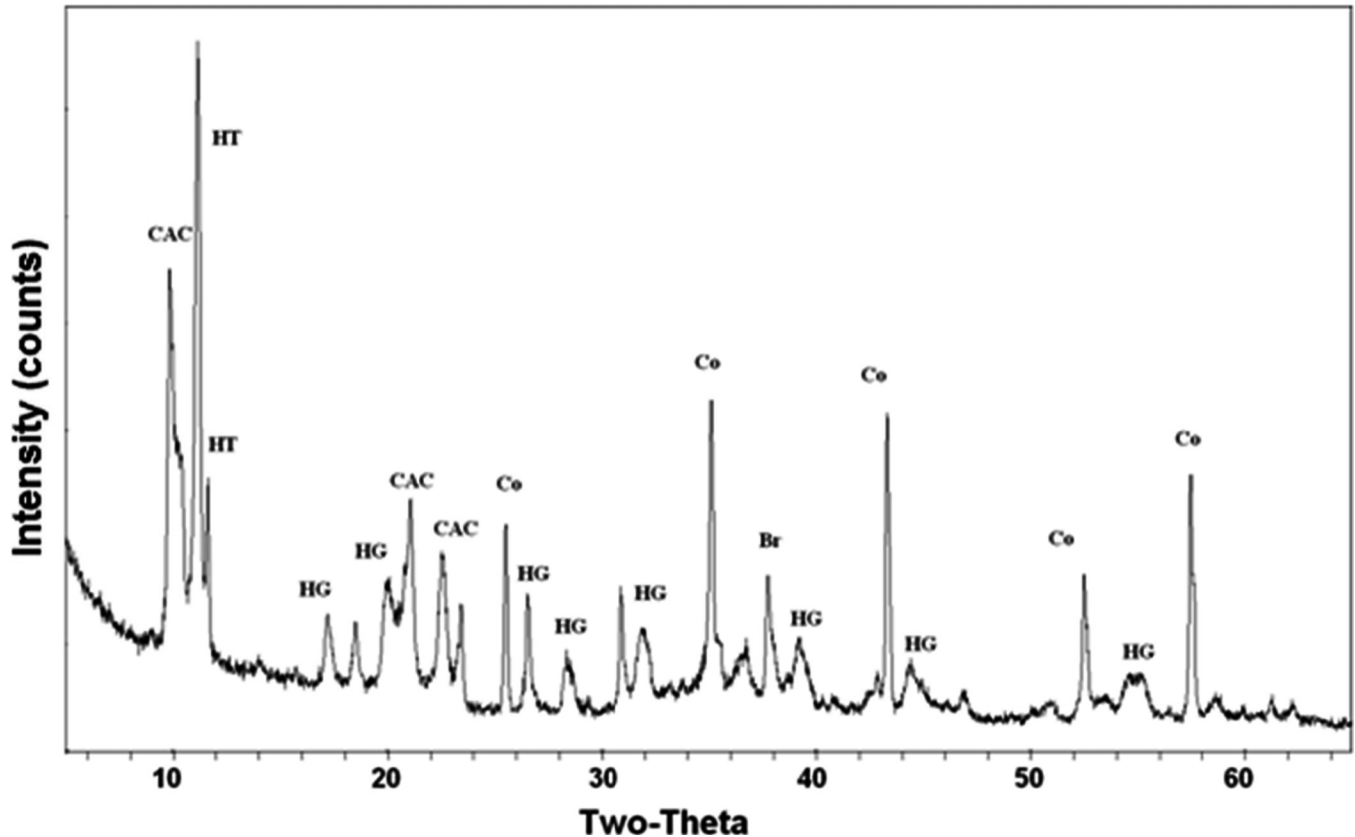


Figure 3. XRD pattern of HB COPR (BM: Brownmillerite; CAC: Calcium Aluminum Chromate 9 or 14; Br: Brucite; HG: Hydrogarnet; Co: Cobalt standard).

quantification. To evaluate this hypothesis, a sample of HB COPR was scanned immediately after preparation, stored in a desiccator, and again scanned seven days later. Results of the second scan showed the maximum peak intensity for CAC and hydroxylite were reduced by at least half while no other peaks gained intensity. A plausible explanation is that as minerals dehydrate crystal quality degrades such that the crystal is less likely to produce a strong XRD peak [37]. Gradual degradation of hydration products may also explain large standard deviations reported in literature regarding mineralogy of HB COPR [4,10].

Another attempt to increase accuracy of HB quantification was to modify the RIR value of hydrated products to better approximate relative quantities for each mineral. The reported RIR value for hydroxylite and CAC-9 are 0.0 and 0.9, respectively [33]. These minerals produce very strong low-angle peaks which are disproportionate to their actual concentration in HB COPR complicating any phase quantification. Chrysochoou *et al.* (2007) compared literature RIR values for CAC minerals and highlighted disparate values reported for similarly structured CAC-9, CAC-12 and CAC-

14 which are 0.9, 1.0, and 3.0, respectively [4,33]. RIR value for the Chrysochoou study was set by determining total chromium content via XRF and determining how much CAC can exist in a given sample of GB COPR. That same methodology was applied to this study. CAC limit was 11.6% w/w measured via XRF calculations and using literature RIR values CAC was 17.7% w/w. The RIR for all CAC phases were made one value and that one RIR was manipulated until calculated CAC weight fell below the feasible CAC limit. RIRs used for all minerals is presented in Table 1.

These methods for improving HB quantification are necessary for quantification of overlapping phases in COPR. Quantification of mineral phases via XRD is less accurate when dealing with multi-phased materials such as COPR and should be regarded as marginally accurate when dealing with such a diverse material as COPR. Multiple lines of evidence towards phase quantification will prevent a mineral from being overrepresented in a particular sample due to an inaccurate RIR value or preferred orientation. Any use of quantitative XRD data of COPR should incorporate supplemental tests to corroborate identified phases.

## Thermogravimetry

Results for TGA analyses are displayed in Figure 3(a) and Figure 3(b). Many GB and HB COPR liberation peaks occur at similar temperatures, specifically at 80°, 200°, 350°, and 700°C, but HB consistently displays greater weight losses at each liberation event thus confirming XRF results that more volatiles exist in HB than in GB. The LOI for GB and HB COPR were 9.9 and 29.6 weight %, respectively. During the TGA test, ion chromatograms for H<sub>2</sub>O and CO<sub>2</sub> were produced (See Figure 5). Major contributors to LOI were H<sub>2</sub>O and CO<sub>2</sub> which comprised over 97% of total liberated ions in both GB and HB COPR. Thus, other volatiles incorporated in COPR minerals are present in trace amounts.

GB and HB COPR produced five separate dehydration events all of which occurred under 400°C. These peaks may be attributed to various hydration products of brownmillerite, mainly LDHs and CACs [36]. Both samples also had measureable loss of H<sub>2</sub>O under 100°C. Due to ambient temperature degradation of HB COPR in the XRD study this likely includes unbound pore water in addition to dehydration of CAC minerals and poorly-formed hydrotalcites. Dehydrations at 80°C, 280–300°C, and the small event at 420°C are attributed to a Mg/Al hydrotalcite [36]. Similar TGA studies suggest the entire dehydration from 100°C to 400°C is from LDHs and Brucite-type sheet clays [35,36]. XRD confirms that LDHs exist in these specimens in the form of hydrogarnet, brucite, and hydrotalcite. Furthermore, increased magnitude of these particular hydration peaks in HB COPR suggests the hydration taking place during weathering of GB COPR produces LDHs in HB COPR such as hydrogarnet, brucite, and CAC.

Two dehydration events not associated with LDHs occurred at 150°C and 350°C. At 150°C a peak occurs in HB that is not replicated in GB. The only known mineral associated with COPR which dehydrates at this specific temperature is chromatite (CaCrO<sub>4</sub>) [35] which was not detected by XRD. Furthermore, chromatite loses additional mass between 500–550°C which is not seen in this TGA analysis [35]. The most likely explanation is an amorphous phase precipitated with pore fluid and retained water. The second event at 350°C was attributed to Portlandite, a phase apparent in the XRD patterns.

Decarboxylation occurred in two distinct events. A small mass loss occurred at 400°C and a larger event occurred between 675°C and 725°C. Calcite and hy-

drotalcite are the only carbon-bearing minerals identified in COPR material and hydrotalcite does not release carbon in the temperature range that this loss observed [36]. Amount of Mg in COPR limits the amount of CO<sub>2</sub> held in hydrotalcite to under 1% bulk weight [38]. Thus, calcite (CaCO<sub>3</sub>) is the likely source of this decarboxylation event. The larger mass loss is attributed to a release of CO<sub>2</sub> from (CaCO<sub>3</sub>). The trailing edge in the decarboxylation mass loss as seen in Figure 4(b) is likely due to poorly crystallized calcite while concentrated mass loss is due to highly crystalline calcite [15]. Material undergoing transition from amorphous to crystalline generally has a lower reaction temperature than highly crystalline material [35] which manifests itself in the larger peak width of the calcite decar-

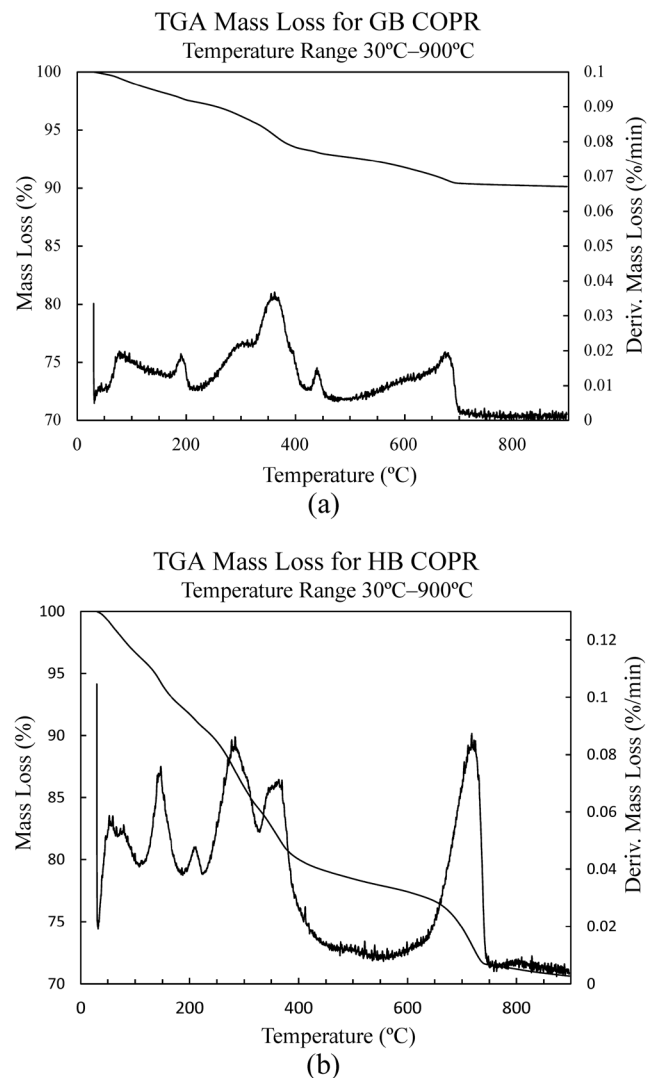


**Figure 4.** (a) Liberation of CO<sub>2</sub> and H<sub>2</sub>O volatiles from GB COPR via TGA during linear temperature ramp from 30°C to 900°C. (b) Liberation of CO<sub>2</sub> and H<sub>2</sub>O volatiles from GB COPR via TGA during linear temperature ramp from 30°C to 900°C.

boxylation. Total loss of CO<sub>2</sub> in GB COPR was 2% by weight. Using stoichiometry the theoretical weight of CaCO<sub>3</sub> in this sample should be 4.5%. This is similar to the XRD results (See Table 3) which indicated a calcite concentration of 3.2% by weight.

### Amorphous Phases

COPR is similar in many respects to Portland cement—basic pH, similar ion composition, and propensity to hydrate [9,15,39]. Similarities between COPR and cement were used to predict types of amorphous phases in COPR because phases of amorphous content were not analyzed directly. A mass balance has been used to create upper bounds for CAC and calcite concentrations and may be applied similarly to estimate amorphous content. Table 4 displays the mass balance of COPR with respect to amorphous material. Mass balance of amorphous content was produced by taking the weight contribution of each oxide determined by XRF and subtracting weight contribution of each mineral phase determined by XRD. Mass not accounted for by the XRD analysis is taken as an amorphous phase. Mass balance was then used to postulate what compounds may exist in amorphous content. Three possible sources of amorphous compounds include:

1. Melted residue from the roasting process
2. Precipitation from leachate
3. Semi-crystallized (gelled) hydration products of brownmillerite

Iron is commonly found as an amorphous phase especially in roast materials such as COPR that have been subjected to high temperatures [1]. FeO(OH), FeO, and ferrihydrite compounds are byproducts in iron-containing materials roasted above 1600°C and may account for a significant fraction of amorphous iron found in this material. Iron oxide granules were observed via SEM but crystal structure was not examined. Amorphous compounds may be an important sink related to transport of Cr(VI). Tinjum *et al.* 2008 discusses implications of chromium adsorption to iron minerals such as goethite and magnetite and although neither magnetite nor goethite were found via XRD chromium adsorption is not dependent on structure. Rather, it is dependent on the valency of iron and pH [25,28]. Goethite and magnetite represent Fe(II) and Fe(III) valence states of iron and both minerals have been found to adsorb chromium by reduction and immobilization [25,28]. Furthermore, magnetite was found to precipi-

tate an iron chromium compound [28]. At the extremely basic pH levels normally associated with COPR (pH = 12.5), precipitation of Cr(III) compounds via magnetite or goethite reduction was predicted to be negligible [40]. Chrysochoou (2009) performed  $\mu$ -XANES analyses on COPR material and found a possible correlation between amorphous iron-rich oxyhydroxides and Cr(VI) hotspots [26].

Calcium compounds which compose the largest fraction of the amorphous content (See Table 4) may originate via pore fluid precipitation and from degradation of brownmillerite. The gradual decarboxylation peak (See Figure 4) in both types of COPR indicates amorphous and semi-crystalline calcite exist. Hydration products of brownmillerite are also a plausible source of amorphous calcium compounds because these transition phases are poorly crystalline. During the hydration process several intermediate products develop most of which are undetectable via XRD [10]. Appreciable amount of CAC and hydrogarnet found in the GB COPR in this study indicates that brownmillerite has undergone some hydration in the GB COPR but a cementation phase characteristic of HB COPR is not prevalent. The large fraction of hydrated products in GB COPR suggests an equally large amount

**Table 4. Mass Balance of GB and HB COPR Crystalline and Amorphous Content (all data reported in wt.%).**

	GB COPR		*Total
	Crystalline	Amorphous	
CaO	26.5	10.4	36.9
Fe <sub>2</sub> O <sub>3</sub>	17.6	4.7	21.3
Al <sub>2</sub> O <sub>3</sub>	9.5	2.4	11.9
MgO	4.6	3.7	8.3
Cr <sub>2</sub> O <sub>3</sub>	1.1	1.8	2.9
SiO <sub>2</sub>	3.5	0.0	3.5
CO <sub>2</sub> /H <sub>2</sub> O	7.5	4.9	12.4
	<b>67.7</b>	<b>26.0</b>	<b>97.2</b>
	HB COPR		*Total
	Crystalline	Amorphous	
CaO	11.2	18.1	29.4
Fe <sub>2</sub> O <sub>3</sub>	3.0	14.9	17.9
Al <sub>2</sub> O <sub>3</sub>	7.4	3.5	11.0
MgO	6.1	0	6.1
Cr <sub>2</sub> O <sub>3</sub>	2.0	0.8	2.8
SiO <sub>2</sub>	0	1.6	1.6
CO <sub>2</sub> /H <sub>2</sub> O	15.8	13.1	28.9
	<b>45.5</b>	<b>52.0</b>	<b>97.7</b>

\*From XRF Analysis

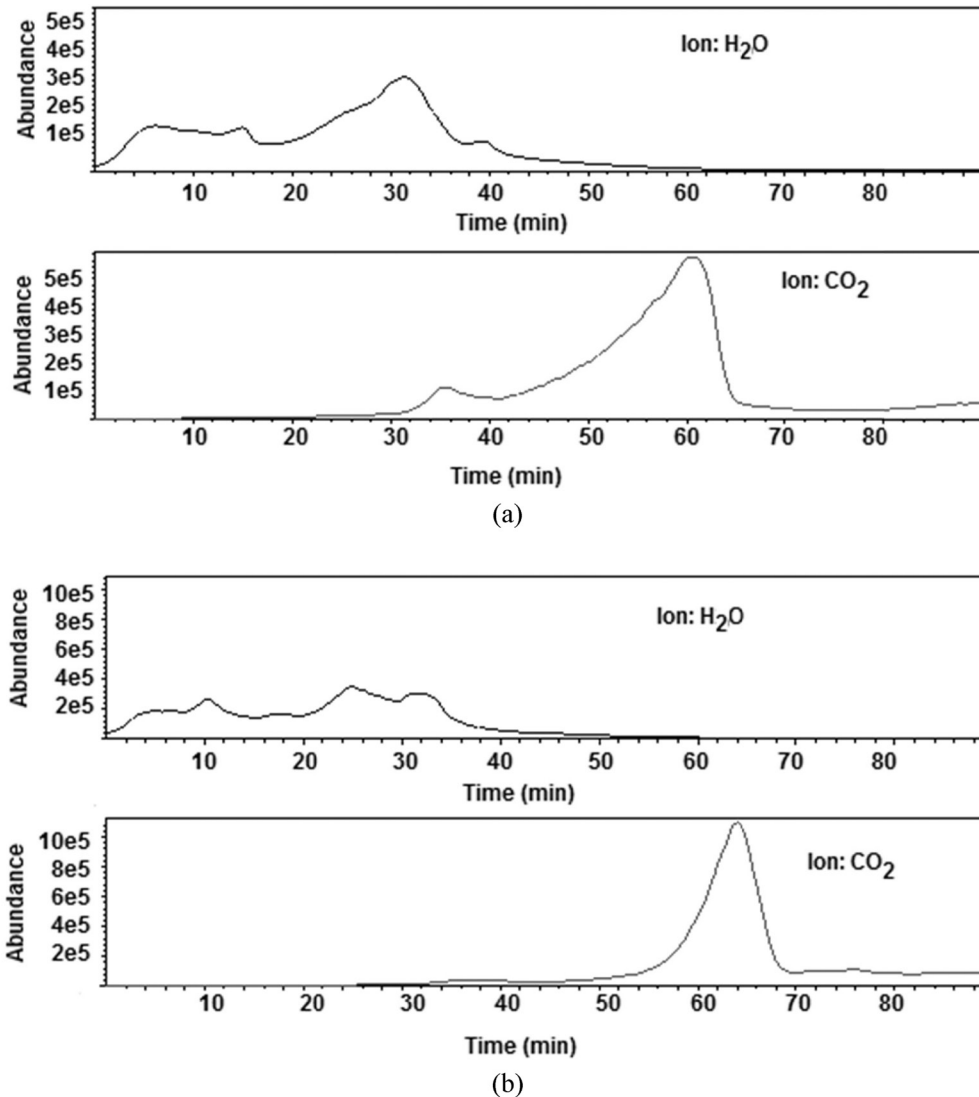


**Figure 5.** Ion chromatograms for  $H_2O$  and  $CO_2$  liberated from COPR samples; (a) GB and (b) HB COPR. Abundance is measured in molecules counted. Note different scale in Figure 3(b).

of amorphous transition phases which likely dominates the amorphous mass.

The study of COPR by multiple and supporting lines of analytical techniques (XRD, XRF, SEM, and TGA) has provided information about crystalline chemistry, amorphous chemistry, and sources of  $H_2O$  and  $CO_2$  in COPR of both the GB and HB variety. This paper has identified and quantified major mineral phases in COPR including brownmillerite and hydrated phases believed to be central in expansion processes of COPR [10,32]. The amorphous phases in COPR which account for approximately half of the material bulk mass include iron oxyhydroxides, intermediate stages of brownmillerite hydration, and semi-crystalline precipitates. At least one class of compounds in the amorphous content, iron oxyhydroxides, has potential to reduce hexavalent

chromium and mitigate leaching. Use of TGA in the study of COPR mineralogy provided an independent and complementary testing method with low user bias. TGA has provided a way to qualify otherwise potentially biased XRD results of COPR by providing limits on mineral abundance based on hydration and carboxylation.

#### ACKNOWLEDGEMENTS

This work was partially funded by Honeywell International and performed at the University of Wisconsin-Madison. Special thanks to John Fournelle and Brian Hess of the University of Wisconsin-Madison Department of Geosciences for their assistance in preparing for and conducting XRD and SEM analyses.

## REFERENCES

- Doerner, "Producing Chromate Salts from Domestic Ores", *Chem. Metall. Eng.* 1940, pp. 688–689.
- Bartlett, R. J.; James, B. R., "Mobility and Bioavailability of Chromium in Soils", In *Chromium in the Natural and Human Environments*; Nieboer, J. O. N. a. E., Ed.; John Wiley & Sons: New York, Vol. 20, 1988, pp. 268–303.
- Environmental Protection Agency. "Technical Factsheet on: Chromium", <http://www.epa.gov/safewater/pdfs/factsheets/ioc/tech/chromium.pdf> (accessed March 2010).
- Chrysochoou, M.; Dermatas, D., "Application of the Rietveld method to assess chromium(VI) speciation in chromite ore processing residue", *J. Hazard. Mater.* Vol. 141, 2007, pp. 370–377.
- Chrysochoou, M.; Dermatas, D.; Moon, D. H.; Christodoulatos, C.; Wazne, M.; French, C.; Morris, J.; Kaouris, M., "Investigation of Barium Treatment of Chromite Ore Processing Residue (COPR)", *J. ASTM* Vol. 3, No. 6. 2006, pp. 1482.
- Thomas, R. P.; Hillier, S. J., "Analytical Characterization of Solid- and Solution-Phase Chromium Species at COPR-Contaminated Sites", *Environ. Geochem. and Health* Vol. 23, No. 3, 2001, pp.195–199.
- Wazne, M.; Papastavrou, M.; Papazoglou, P.; Meng, X.; Dermatas, D.; Christodoulatos, C.; Moon, D. H.; Kaouris, M.; Morris, J.; Jackson, R. L., "Leaching Behavior of Chromite Ore Processing Residue", In *In situ and On-Site Bioremediation—2005: Proceedings of the Eighth International In situ and On-Site Bioremediation Symposium*; Battelle Press: Baltimore, Maryland, 2005, pp. 8.
- Moon, D. H.; Wazne, M.; Dermatas, D.; Christodoulatos, C.; Sanchez, A. M.; Grubb, D. G.; Chrysochoou, M.; Kim, M. G., "Long-term treatment issues with chromite ore processing residue (COPR): Cr<sup>6+</sup> reduction and heave", *J. Hazard. Mater.*, Vol. 143, 2007, pp. 629–635.
- Dermatas, D.; Chrysochoou, M., "Current Knowledge on Heaving Mechanisms of Chromite Ore Processing Residue (COPR)", *GeoCongress 2008: Geotechnics of Waste Management and Remediation* 2008.
- Dermatas, D.; Chrysochoou, M., "Mineralogical Characterization of Chromite Ore Processing Residue at Dundalk Marine Terminal Area 1800", 2005.
- Darrie, G., "Commercial Extraction Technology and Process Waste Disposal in the Manufacture of Chromium Chemicals from Ore", *Environ. Geochem. Health*, Vol. 23, 2001, pp. 187–193.
- Moon, D. H.; Dermatas, D.; Sanches, A. M.; Chrysochoou, M.; Wazne, M.; Grubb, D. G., "Assessment of Brownmillerite and Periclase Hydration in Chromite Ore Processing Residue at Elevated Temperature", *GeoCongress 2008: Geotechnics of Waste Management and Remediation (GSP 177)*, New Orleans, 2008, pp. 375–382.
- Meller, N.; Hall, C.; Crawshaw, J., "ESEM evidence for through-solution transport during brownmillerite hydration", *J. Mat. Sci.*, Vol. 39, 2004, pp. 6611–6614.
- Dermatas, D.; Chrysochoou, M.; Moon, D. H.; Grubb, D. G.; Wazne, M.; Christodoulatos, C., "Ettringite-Induced Heave in Chromite Ore Processing Residue (COPR) upon Ferrous Sulfate Treatment", *Environ. Sci. Technol.*, Vol. 40, 2006, pp. 5786–5792.
- Dweck, J.; Ferreira da Silva, P. F.; Buchler, P. M.; Cartledge, F. K., "Study by Thermogravimetry of the Evolution of Ettringite Phase During Type II Portland Cement Hydration", *J. Therm. Anal. Calorim.*, Vol. 69, 2002, pp. 179–186.
- Weng, C. H.; Huang, C. P.; Sanders, P. F., "Effect of pH on Cr(VI) Leaching from Soil Enriched in Chromite Ore Processing Residue", *Environ. Geochem. and Health*, Vol. 23, 2001, pp. 207–211.
- Millsbaugh, A.; Tinjum, J.; Boecher, T. A., "Specific Gravity of Expansive Chromium Ore Processing Residue with Complex Microstructure", *ASTM*, Vol. 33, 2010, pp. 309–316.
- Tinjum, J.; Houck, C.; French, C., "Field Investigation Techniques for Characterization and Delineation of COPR", *GeoCongress 2008: Geotechnics of Waste Management and Remediation*, New Orleans, Louisiana, 2008.
- Hillier, S.; Roe, M. J.; Geelhoed, J. S.; Fraser, A. R.; Farmer, J. G.; Paterson, E., "Role of quantitative mineralogical analysis in the investigation of sites contaminated by chromite ore processing residue", *Sci. Total Environ.*, Vol. 308, 2003, pp. 195–210.
- Chrysochoou, M.; Fakra, S. C.; Marcus, M. A.; Moon, D. H.; Dermatas, D., "Microstructural Analyses of Cr(VI) Speciation in Chromite Ore Processing Residue (COPR)", *Environ. Sci. Technol.*, Vol. 43, 2009, pp. 5461–5466.
- Weng, C. H.; Huang, C. P.; Allen, H. E.; Cheng, A. H.-D.; Sanders, P. F., "Chromium leaching behavior in soil derived from chromite ore processing waste", *Sci. Total Environ.*, Vol. 154, 1994, pp. 71–86.
- Ignaz, J.; Hug, G. a. S. J., "Influence of Mineral Surfaces on Chromium(VI) Reduction by Iron(II)", *Environ. Sci. Technol.*, Vol. 33, 1999, pp. 4285–4291.
- MacNaughton, M. G., "Adsorption of chromium(VI) at the oxide water interface", *Biological Implications of Metals in the Environment*, Springfield, VA, 1977, pp. 240–253.
- Tinjum, J. M.; Benson, C. H.; Edil, T. B., "Mobilization of Cr(VI) from Chromite Ore Processing Residue through acid treatment", *Sci. Total Environ.*, Vol. 391, 2008, pp. 13–25.
- Chrysochoou, M.; Fakra, S. C.; Marcus, M. A.; Moon, D. H.; Dermatas, D., "Microstructural Analyses of Cr(VI) Speciation in Chromite Ore Processing Residue (COPR)", *Environ. Sci. Technol.*, Vol. 43, 2009, pp. 5461–5466.
- Kamolpornwijit, W.; Meegoda, J. N.; Hu, Z., "Characterization of Chromite Ore Processing Residue", *Periodical of Haz., Toxic, and Radioactive Waste Mgmt.*, Vol. 11, No. 4, 2007, pp. 234–239.
- Asmundson, K., "Transport of hexavalent chromium in the vadose zone by capillary and evaporative transport from Chromium ore processing residue fill", *Environ. Sci. Technol.* 2011, (under review).
- Deng, Y.; Stjernstrom, M.; Banwart, S., Accumulation and remobilization of aqueous chromium(VI) at iron oxide surfaces: Application of a thin-film continuous flow-through reactor", *J. Contam. Hydrol.*, Vol. 21, 1996, pp. 141–151.
- Meegoda, J. N.; Kamolpornwijit, W.; vaccari, D. A.; Ezeldin, A. S.; Novak, B. A.; Mueller, R. T.; and Santora, S., "Remediation of Chromium-Contaminated Soils: Bench-Scale Investigation", *Periodical of Haz., Toxic, and Radioactive Waste Mgmt.*, Vol. 3, No. 3, 2003, pp. 124–131.
- CHEMEX, "A Standard Method for X-Ray Fluorescence with the Whole Rock Analytical Method", 2009.
- Dermatas, D.; Chrysochoou, M., "Influence of X-Ray Diffraction Sample Preparation on Quantitative Mineralogy: Implications for Chromate Waste Treatment", *J. Environ. Qual.*, Vol. 36, 2007, pp. 487–497.
- Chrysochoou, M.; Moon, D. H.; Dermatas, D.; Wazne, M.; Christodoulatos, C.; Meng, X.; Kaouris, M.; Morris, J.; French, C.; Sass, B. M., "Mineralogical Analysis of Chromite Ore Processing Residue by X-Ray Powder Diffraction"; Stevens Institute of Technology: Hoboken, New Jersey, 2005.
- Inorganic Crystal Structure Database (ICSD). 2009.
- Carnahan, J. Thermogravimetric Analysis Report and Summary. 2009.
- Clark, R. P.; Gallagher, P. K.; Dillard, B. M., "Thermoanalytical investigation of calcium chromate", *Thermochim. Acta*, Vol. 33, 1979, pp. 141–155.
- Chmielarz, L.; Kustrowski, P., "Influence of Cu, Co, and Ni cations incorporated in brucite-type layers on thermal behaviour of hydrotalcites and reducibility of the derived mixed oxide systems", *Thermochim. Acta*, Vol. 395, 2003, pp. 225–236.
- Cullity, B. D. and Stock, S. R. 2001. *Elements of X-Ray Diffraction*, 3rd ed., Upper Saddle River, NJ: Prentice Hall.
- WebMineral. <http://webmineral.com/data/Hydrotalcite.shtml> (accessed Jan 19, 2010).
- Linnu, L.; Yongjia, H., "Structural Characteristics of Dehydrated Phase of Hardened Cement Paste and its Rehydrating Ability", *J. Chinese Ceramic Soc.*, Vol. 36, No. 10, 2008, pp. 1343–1347.
- Sposito, G. 1989. *The Chemistry of Soils*; New York, NY: Oxford University Press.



# Oil Removing Technology of Residues from Waste Oil-based Drilling Fluid Treated by Solid-liquid Separation

BING HOU<sup>1,\*</sup>, CHUAN LIANG<sup>2</sup>, HAO DENG<sup>2</sup>, SHUIXIANG XIE<sup>3</sup>, MIAN CHEN<sup>3</sup> and RONGSHA WANG<sup>3</sup>

<sup>1</sup>State Key Laboratory of Petroleum Resource and Prosecting, China University of Petroleum (Beijing), Beijing, China, 102249

<sup>2</sup>College of Petroleum Engineering, China University of Petroleum (Beijing), Beijing, China, 102249

<sup>3</sup>CNPC Research Institute of Safety & Environment Technology, Beijing, China, 100083

**ABSTRACT:** Oil base drilling fluid has received increasing attention due to its use in deep wells and complex well drilling operations. However, it produces a considerable amount of environmental pollution while drilling operations are completed. Solid-liquid separation is one of the most widely used technologies for pretreating waste oil-based drilling fluid. When waste oil-based drilling fluid is pretreated by this technology liquid phase may be used to reconfigure oil-based drilling fluid. However, innocent treatment has to be carried out on remaining residue (i.e., oily cuttings) to meet well field environmental concerns. Technologies for processing oily cuttings such as bioremediation, de-emulsification, and landfill freezing have been studied at home and abroad. Each method has certain limitations such as a long biological repair time, high demand for landfill sites, critical conditions for freezing, and potential secondary pollution produced by de-emulsifying. This work seeks to describe a highly efficient degreasing agent named CYJ-12 developed based on characteristics of oily cuttings. Oil removal from oily cutting surfaces and harmless disposal of oily cutting were accomplished by concerted actions of an anionic surfactant, a non-ionic surfactant, solvents, and a soft agent in combination with advanced separation equipment. Oil removal rate reached more than 90%. The oil removal mechanism of CYJ-12 was analyzed using infrared spectroscopy, gas chromatography, and liquid chromatography.

## INTRODUCTION

**T**HE number of branch wells and horizontal wells is increasing in oil and gas exploration and in the development process. Decreasing sidewall stability is gradually becoming problematic and more oily cuttings have been produced. Oil-based drilling fluid technology has attracted increased attention. It is urgent at the same time to develop harmless handling technologies for waste oil-based drilling fluid. Some countries have strict regulations on oil content of oily cuttings. Oily material content of solid waste has been mandated in Europe since 1993 and zero emissions have been required since November 2000. Technologies for oily cutting processing such as bioremediation, landfill freezing, solid-liquid separation, supercritical fluid extraction, and microwave pyrolysis have been studied in the literature with various limitations.

\*Author to whom correspondence should be addressed.  
E-mail: houbing9802@163.com

## Bioremediation Method

Sums of experiments on bioremediation of oily cuttings were conducted in Indonesia. Microorganisms and oily cuttings were mixed regularly. Content and chemical composition of hydrocarbons and their nutrient concentrations and microorganism quantities were monitored periodically. Results of analysis have suggested bioremediation may address discarded oil base drilling fluid. However, processing time of bioremediation was often more than seven days and processing effect for high oil content of oily cuttings was poor [2,3,7].

## De-emulsifying Method

The main application for de-emulsification used a chemical broken agent A and water was added to emulsify oily cuttings. Oil could be separated from oily cuttings with an addition of chemical and other methods. Although these methods have different effects, chemi-



cal additives would improve cost, increase complexity of drilling fluid composition, and have negative effects on the environment [1,5,8,9,10,11].

### Injection Formation Method

After oil drilling cuttings were smashed they were injected into strata through a borehole or kept in the borehole annular space. This method not only had strict requirements regarding strata but also for equipment. Treatment cost in addition was higher and valuable mineral oil resources were wasted. Therefore, this method poses a potential environmental pollution hazard.

Thus, need to develop a highly efficient and economical method for processing oily cuttings is urgent. Past analysis of existing processing technologies and results from indoor experiments indicated a chemical strengthening separation method may process oily cuttings with help from an efficient degreasing agent and a centrifuge separation. Oil in a liquid may be recovered after centrifuge separation and the water phase may be reused for oily cuttings [4,6] providing a new way to resolve environmental pollution resulting from oily cuttings.

## MATERIALS AND METHODS

### Experimental Instruments and Materials

Reagents were used. Main experimental reagents included ethylenediaminetetraacetic acid tetrasodium salt (chemical pure), dodecyl sodium sulfate sodium (chemical pure), sodium lauryl ether sulfate (chemical pure), n-butanol (chemical pure), Tween 80 (chemical pure), glycerol monooleate (chemical pure), butyl lactate (chemical pure), petroleum ether (analytical pure), carbon tetrachloride (analytical pure), anhydrous sulfate sodium (analytical pure), sodium chloride (analytical pure), and hydrochloric acid (analytical pure).

Lab instruments were also used. Instruments included a cracking gas chromatograph (Shimadzu, Japan), a gas chromatograph-mass spectrometer (Agilent, American), a top air-ms analysis instrument (Agilent, American), a Fourier infrared spectrometer (Thermo Nicolet, American), a mass spectrometer (Waters, American), an element analyzer (China), a high performance liquid chromatograph, an oil480 infrared measuring oil meter (China), a high temperature furnace (China), an oven (China), an electronic balance (China), and a small centrifuge (China).

### Experimental Method

#### *Preparation of Highly Efficient Degreasing Agent CYJ-12*

1. A total of 30 ml of water was heated to approximately 60°C and then 0.2 g EDTA-2Na was added. After EDTA-2Na dissolution, 7 g dodecyl sodium sulfate sodium was slowly added while stirring. After completely dissolving, 15 g sodium lauryl ether sulfate (SLES) was added slowly while stirring. Then, 0.2 g n-butanol was added while stirring.
2. A total of 3 g hard alcohol lactic ester, 10 g Tween 80, and glycerol monooleate were added to 12 g butyl lactate while stirring to dissolve. Then, the solution was heated to 60°C with a water bath.
3. Mixture (1) was added to mixture (2) slowly while stirring to dissolve.
4. A total of 0.1 g potassium hydroxide and 0.2 g EDTA were added into mixture (3) while stirring.
5. After the solution became transparent, the preparation process was complete.

#### *Determination of Oil Content of Oily Cuttings Before Treatment*

Twenty-gram (accurate to 0.1 g) samples of oily cuttings were measured. Then, 100 ml anhydrous petroleum ether (90–120°C) was added. Moisture determination was connected and backflow speed was controlled at 2–4 drops/second. Once the volume of water in the receiving device no longer increased heating was stopped. The sample was cooled and volume of water was noted. The fluid in the bottle was cooled with distillation and then suction filtered using a Buchner funnel equipped with heavy filter paper. After suction finished the filter residue was dried at  $105 \pm 3^\circ\text{C}$ . Quantity of oil was measured using the reduction method and then oil content of oily cuttings determined.

#### *Determination of the Oil content of Oily Cuttings After Treatment*

Twenty-gram samples of cuttings were measured accurately by an electronic balance. A total of 20 ml carbon tetrachloride was added and the mixture was repeatedly shaken. Diluted hydrochloric acid (i.e., strong hydrochloric acid diluted with 5 parts water) was added to the solution to make the pH value less

**Table 1. Component and Heavy Metal Content of Oily Cuttings from Daqing Oil Fields.**

Samples	Water Content (wt,%)	Oil Content (wt, %)				Solid Content (wt, %)
	11.5	6.5				82.0
Oily cuttings	Heavy Metal Content (mg/kg)					
	Hg	As	Cr	Pb	Cd	Mineral oil
	1.5	13.6	19.2	0.18	0.11	65,000
GB8248-84 "control standards of agricultural sludge pollutants"	15	75	1,000	1,000	20	3,000

than 2. Next, sodium chloride was added to the solution. The sample was oscillated for 30 minutes. Then, the fluid from the tapered bottle was poured into a glass separating funnel. After stratification, the bottom liquid of the tapered bottle was filtered through a sand core glass funnel and then poured into a volumetric flask. The solid phase of the tapered bottle was extracted several times with carbon tetrachloride. After flowing into a 250-ml volumetric flask capacity was measured by carbon tetrachloride. Carbon tetrachloride served as a blank solution and a 4-cm cuvette was used. Petroleum content of the extraction liquid was measured with an oil480 infrared measuring oil meter.

## RESULTS AND DISCUSSION

### Analysis of Oil and Heavy Metal Content of Oily Cuttings

Oily cuttings from the Daqing oilfield were selected. Components and heavy metals contents from oil drilling cuttings were determined and are displayed in Table 1. No specific emissions standards for oily cuttings either at home or abroad were located. Therefore, test results referred to "control standards of agricultural sludge pollutants" (GB 4284-84).

Displayed in Table 1 the main pollutant from oily cuttings from the Daqing oilfield is from mineral oil and other pollutants detected are considered to be in a standard range. Therefore, these samples meet requirements for "control standards of agricultural sludge pollutants" (GB 4284-84) and it allows for harmless disposal of processing or recovery oil.

### Influence of Added Amount of Degreasing Agent CYJ-12 on Degreasing Effect

CYJ-12 and water were mixed in a certain volume ratio to make a degreasing agent solution. Then, oily cuttings were added to form a homogeneous mixture. The mixture sat for 10 minutes and then was separated in the centrifuge. Oil content of the drilling cuttings was determined after centrifugal separation.

Degreasing effect of different amounts of CYJ-12 (i.e., 20,000 mg/L, 4,000 mg/L, 2,000 mg/L, 1,000 mg/L, 500 mg/L, 400 mg/L, 200 mg/L, 100 mg/L, and 50 mg/L) was investigated.

#### Experimental conditions:

Temperature: 25°C

Centrifugal speed: 1,000 r/min

Centrifugal time: 5 minutes

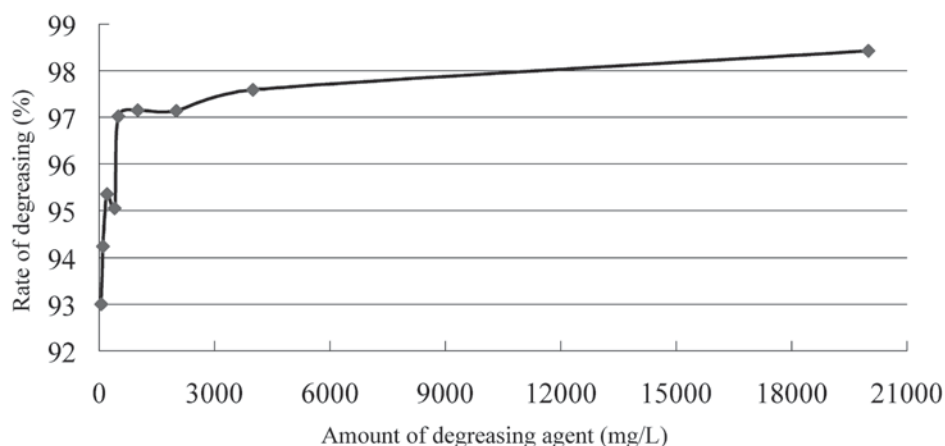


**Figure 1.** Influence of amount of degreasing agent CYJ-12 on degreasing effect.

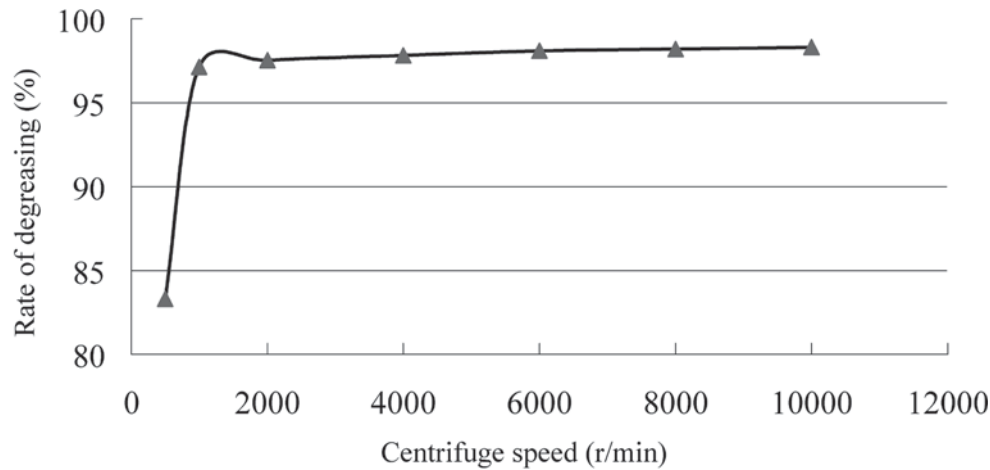


Figure 2. Influence of centrifuge speed on degreasing effect.

Results are provided in Figure 1. CYJ-12 may remove oil from the surface of oily cuttings at a degreasing rate greater than 93%. Degreasing rate increases when CYJ-12 quantity increases. When amount of CYJ-12 added is above 1,000 mg/L degreasing rate increases slightly. Therefore, 1,000 mg/L is an optimal amount to be added.

#### Influence of Centrifugal Centrifuge Speed on the Degreasing Effect

Degreasing effect of different centrifuge speeds (1,000 r/min, 2,000 r/min, 5,000 r/min, 5,500 r/min, 8,000 r/min, and 10,000 r/min) was investigated.

##### Experimental conditions:

Temperature: 25°C  
 Added amount of CYJ-12: 1,000 mg/L,  
 Centrifugal time: 5 minutes

Figure 2 displays an observation that as centrifugal centrifuge speed increases degreasing rate increases. Degreasing rate is stable when centrifuge speed is above 2,000 r/min. Increased centrifuge speed does not significantly increase oil removal effect. Therefore, 2,000 r/min is an optimal centrifuge speed.

#### Influence of Temperature on the Degreasing Effect

Temperature is another vital factor contributing to degreasing effect. Degreasing effect of CYJ-12 under 25°C, 40°C, 50°C, 60°C, 70°C, and 80°C was investigated.

##### Experimental conditions:

Amount of CYJ-12 added: 1,000 mg/L  
 Centrifugal speed: 2,000 r/min  
 Centrifugal time: 5 minutes

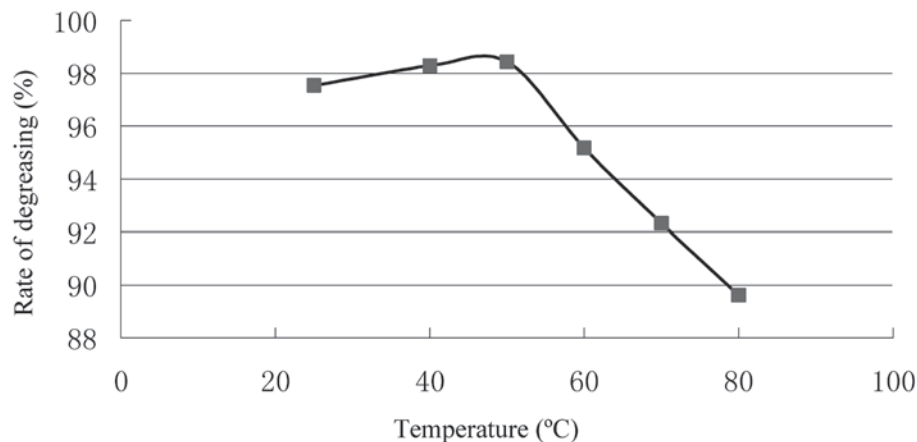
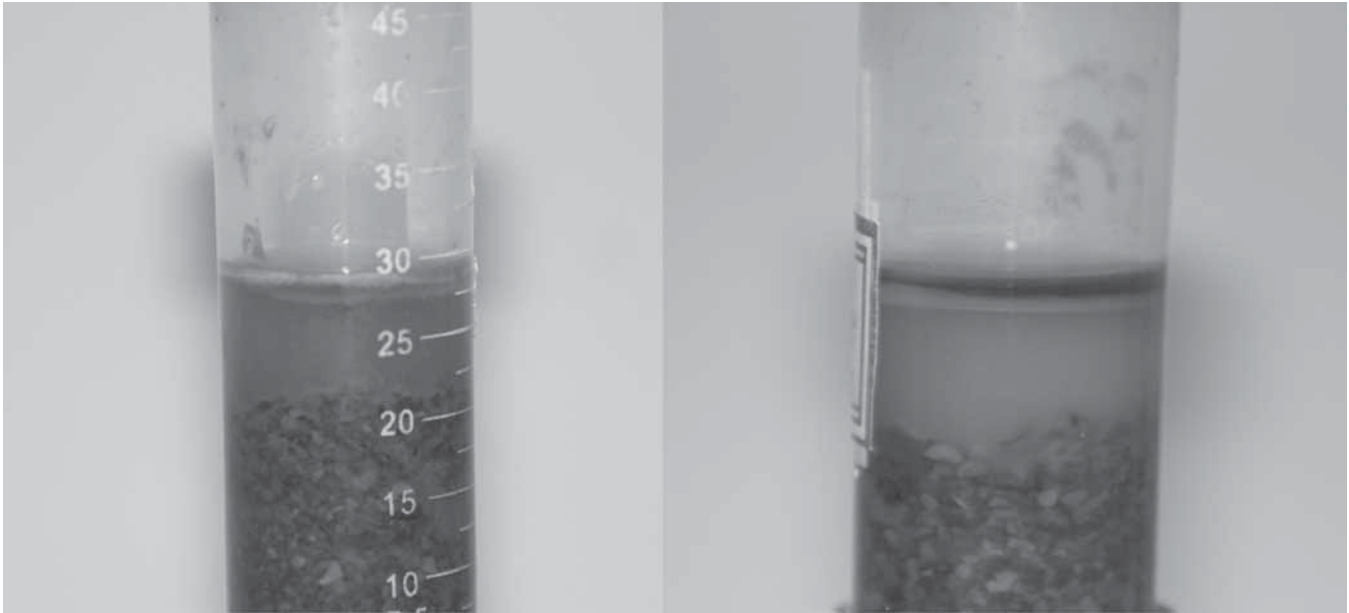


Figure 3. Influence of temperature on degreasing effect.



**Figure 4.** Centrifugation of oily cuttings with and without addition of degreasing agent CYJ-12. (Left is water and cuttings and right is degreasing agent CYJ-12 and cuttings).

CYJ-12 may remove oil from the surface of oily cuttings at a degreasing rate greater than 93% as displayed in Figure 3 and as temperature increases degreasing rate increases. When temperature is more than 50°C degreasing rate decreases slightly. Volatile components of CYJ-12 become more volatile with increasing temperature resulting in a lower effective concentration and decreased interaction between the degreasing agent and oily cutting surface.

Figures 4 and 5 display three phases (i.e., oil, water,

and drilling cuttings) and were stratified after adding CYJ-12. Therefore, oil recovery and reuse of degreasing agents is possible compared to other oil removal performances of currently available industry products and it meets requirements of emissions standards for drilling cuttings.

Degreasing effects of CYJ-12, CPF-168 (Bossdun, USA), and AP113 (Hubei, China) on oily cuttings have been compared to better understand the degreasing effect of CYJ-12.

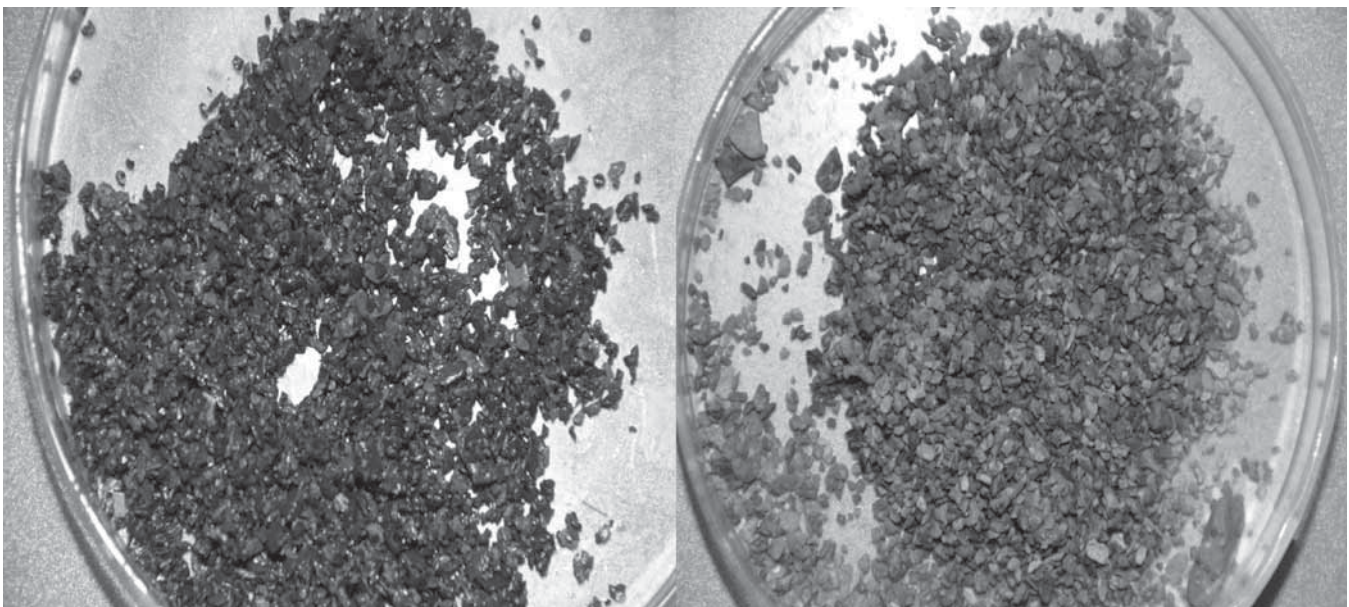


**Figure 5.** Oily cuttings before and after oil removal. (Left is oily cuttings before oil removal and right is oily cuttings after oil removal).

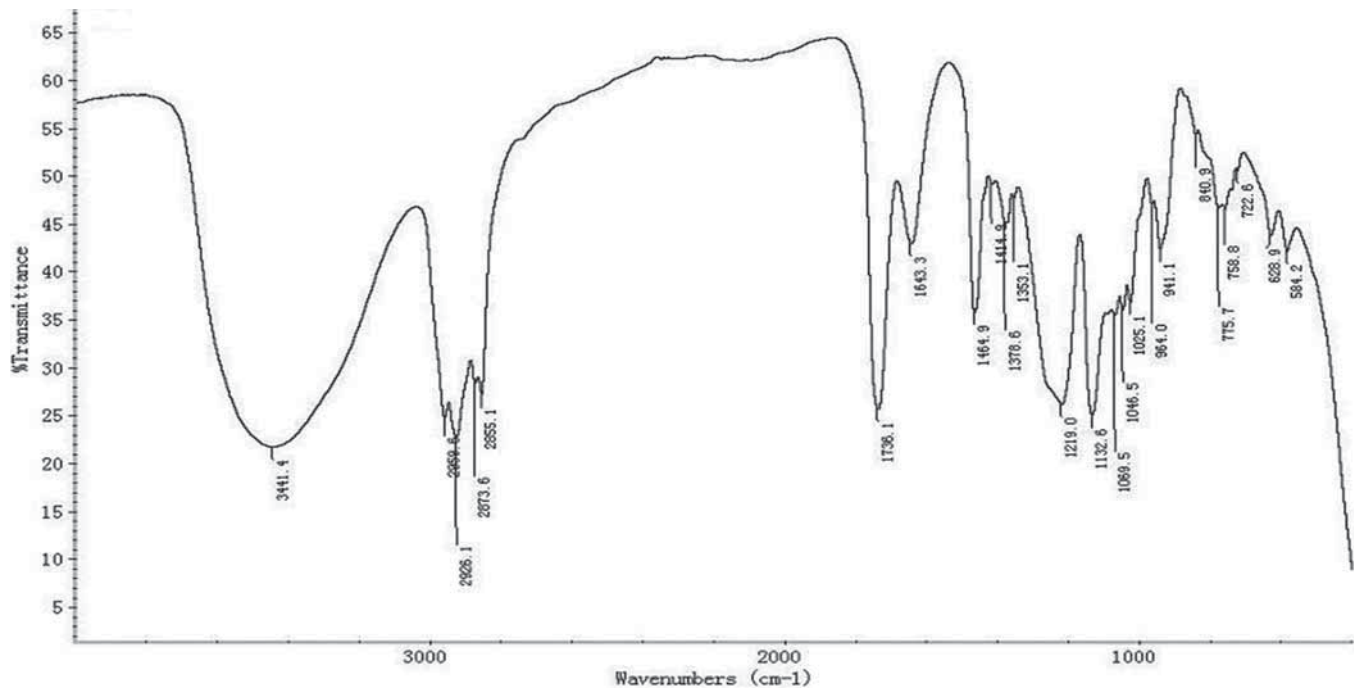


Figure 6. Infrared spectrum of degreasing agent CYJ-12.

#### Experimental conditions:

Sample weight: 1,000 mg/L  
 Temperature: 50°C  
 Centrifugal speed: 2,000 r/min  
 Centrifugal time: 5 minutes

Results are provided in Table 3 indicating degreasing effects from CYJ-12 are superior to CPF-168 and AP113 which meets requirements for waste disposal and resource reclamation on drilling-operation fields.

#### Mechanism of Degreasing Agent CYJ-12

##### Structural Analysis of Degreasing Agent CYJ-12

A Fourier infrared spectrometer, a cracking gas chromatograph, a high performance liquid chromatograph, and other analytical instruments were used to analyze degreasing agent CYJ-12 as displayed in Figures 6, 7, and 8. Degreasing agent CYJ-12 contains C=O, C-O, -OH,  $-\text{SO}_4^{2-}$ ,  $-\text{CH}_2$ ,  $-\text{CH}_3$ ,  $-(\text{CH}_2)_n$ , and  $n > 4$  functional groups. Ether, alcohols, and sulfate

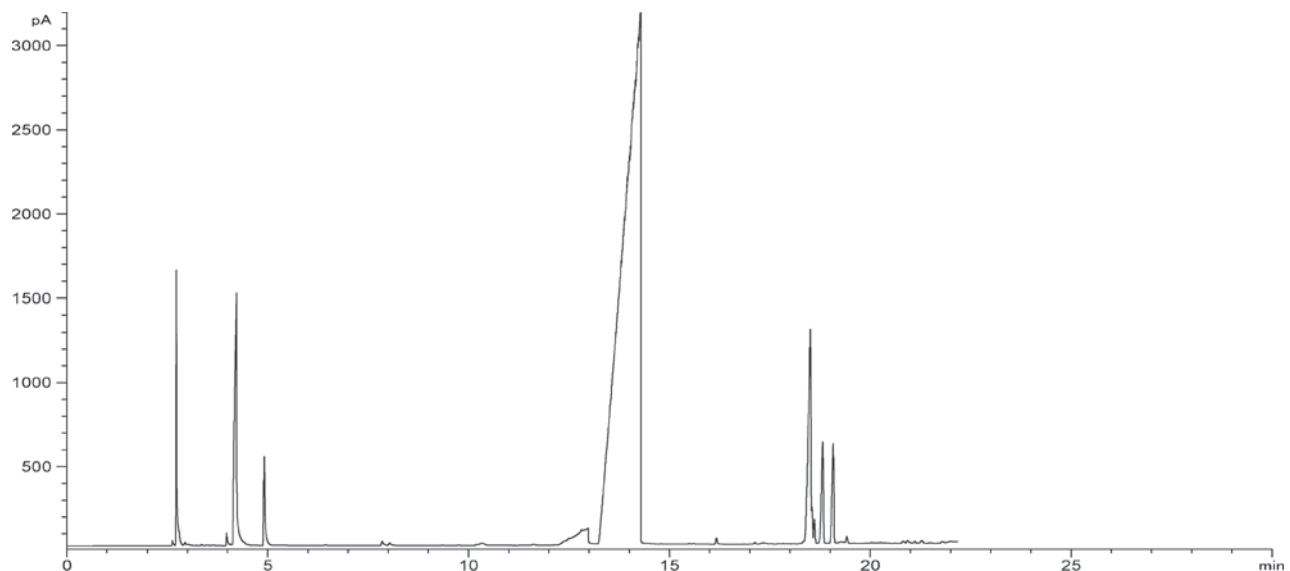


Figure 7. Cracking gas chromatography spectrum of degreasing agent CYJ-12.

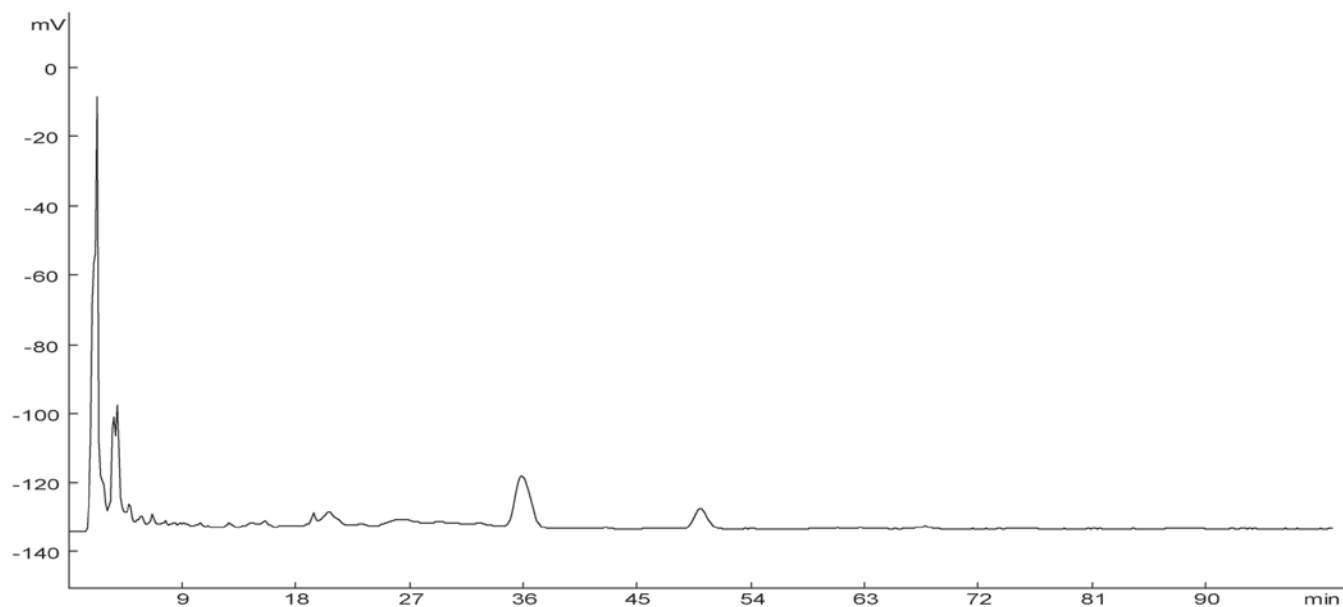


Figure 8. High performance liquid chromatography spectrum of degreasing agent CYJ-12.

may exist. A biodegradable anionic surfactant with a high HLB (Hydrophile-Lipophile Balance Number) value contributes to cleaning and to the environmental protection ability of the degreasing agent. Additionally, a non-ionic surfactant with a low HLB value should be used for its oil emulsion and cleaning abilities.

#### Element Analysis of the Degreasing Agent CYJ-12

Elements of CYJ-12 were analyzed using an element analyzer and are displayed in Table 2. Main elements of the degreasing agent CYJ-12 are C, H, O, and S in addition to a small amount of K and N. The K and N content resulted from adding KOH and EDTA to regulate pH and soften the water, respectively. A soft agent was added to complex calcium magnesium ions in water making the degreasing agent colorless and transparent. pH value of CYJ-12 was also adjusted to be neutral to prevent corrosion of metal equipment.

Table 2. Element Analysis of Degreasing Agent CYJ-12.

Samples	Element Content							
	C %	H %	O %	S %	N ppm	Na %	K ppm	Ca ppm
CYJ-12	43.20	9.15	40.60	2.66	< 1	2.18	116	17

#### Analysis of Oil Removal Mechanism of Degreasing Agent CYJ-12

Surfactants contribute significantly to oil removal due to their emulsion properties. Anionic and non-ionic surfactants are suitable for removing oil. Anionic surfactants such as dodecyl sodium sulfate sodium and SLES have strong emulsifying abilities and may effectively remove smudges but have poor hard water resistance. Non-ionic surfactants such as hard alcohol lactic ester and glycerin mono-fatty acid ester have no strict water hardness requirements. Coordinating their use may facilitate a desired association effect. HLB values of dodecyl sodium sulfate sodium and SLES are 40.0 and 11.7, respectively. Three types of non-ionic surfactants have different HLB values and allow for good oil emulsion and solubilization. In synergy with an anionic and non-ionic surfactant CYJ-12 has a high degreasing effect.

Table 3. Contrast Evaluation of Oil Removal Performances Between Highly Efficient CYJ-12 and Available Industry Products.

Samples	Oil Content Before Treating (mg/L)	Oil Content After Treating (mg/L)	Oil Removal Efficiency (%)
Oil cuttings		65000	
Oil cuttings + CYJ-12	65000	910	98.6
Oil cuttings + CPF-168		6955	89.3
Oil cuttings + AP113		15795	75.7

## CONCLUSIONS

1. Oily cuttings are produced in oil-based drilling fluid the main pollutant of which is mineral oil. Processing and recycling of oil from cuttings are both effective approaches to realizing harmless disposal of oily cuttings.
2. Based on characteristics of oily cuttings a highly efficient degreasing agent named CYJ-12 has been developed. Oil removal from an oily cutting surface and harmless disposal oily cutting were accomplished by concerted actions of an anionic surfactant, a non-ionic surfactant, solvents, and a soft agent in combination with advanced separation equipment providing an oil removal rate of greater than 90%. Results of contrast of CYJ-12 with other available industry products indicate CYJ-12 is a good choice for oil removal performance for artesian wells.
3. An oil removal mechanism of CYJ-12 was studied using infrared spectroscopy, gas chromatography, elemental analysis, and other tests providing important information for improving oil removal performance and researching new degreasing agents for processing oily cuttings.

## ACKNOWLEDGEMENTS

The Authors are grateful for the Project Support by NNSF of China (No. 51204195, No. 51074171, No. 51174217, No. 51234006) and The Project Supported by the Foundation for Innovative Research Groups of the NNSF of China (No. 51221003).

## REFERENCES

1. Bensadok, K., Benammar, S., Lapicque, F., and Nezzal, G. 2008. Electrocoagulation of cutting oil emulsions using aluminium plate electrodes. *Journal of Hazardous Materials*. 152: 423–430.
2. Chaillan, F., Chaîneau, C.H., Point, V., Saliot, A., and Oudot, J. 2006. Factors inhibiting bioremediation of soil contaminated with weathered oils and drill cuttings. *Environmental Pollution*. 144: 255–265.
3. Chaîneau, C.H., Rougeux, G., Yéprémian, C., and Oudot, J. 2005. Effects of nutrient concentration on the biodegradation of crude oil and associated microbial populations in the soil. *Soil Biology and Biochemistry*. 37: 1490–1497.
4. Filippov, L., Thomas, F., Filippova, I., Yvon, J., and Morillon-Jeanmaire, A. 2009. Stabilization of NaCl-containing cuttings wastes in cement concrete by in situ formed mineral phases. *Journal of Hazardous Materials*. 171: 731–738.
5. Ji, G.D., Yang, Y.S., Zhou, Q., Sun, T., and Ni, J.R. 2004. Phytodegradation of extra heavy oil-based drill cuttings using mature reed wetland: an in situ pilot study. *Environment International*. 30: 509–517.
6. Leonard, S. A., and Stegemann, J. A. 2010. Stabilization/solidification of petroleum drill cuttings. *Journal of Hazardous Materials*. 174: 463–472.
7. Mojtahid, M., Jorissen, F., Durrieu, J., Galgani, F., Howa, H., Redois, F., and Camps, R. 2006. Benthic foraminifera as bio-indicators of drill cutting disposal in tropical east Atlantic outer shelf environments. *Marine Micropaleontology*. 61: 58–75.
8. Robinson, J.P., Kingman, S.W., Snape, C.E., Barranco, R., Shang, H., Bradley, M.S., and Bradshaw, S.M. 2009. Remediation of oil-contaminated drill cuttings using continuous microwave heating. *Chemical Engineering Journal*. 152: 458–463.
9. Robinson, J.P., Kingman, S.W., and Onobrakpeya, O. 2008. Microwave-assisted stripping of oil contaminated drill cuttings. *Journal of Environmental Management*. 88:211–218.
10. Shang, H., Snape, C.E., Kingman, S.W., and Robinson, J.P. 2006. Microwave treatment of oil-contaminated North Sea drill cuttings in a high power multimode cavity. *Separation and Purification Technology*. 49: 84–90.
11. Talbi, Z., Haddou, B., Bouberka, Z., and Derriche, Z. 2009. Simultaneous elimination of dissolved and dispersed pollutants from cutting oil wastes using two aqueous phase extraction methods. *Journal of Hazardous Materials*. 163: 748–755.

# Survival of *Ascaris* Ova in Desert Soils: A Risk Assessment

DAVID L. WILLIAMS, IAN L. PEPPER and CHARLES P. GERBA\*

*Department of Soil, Water, and Environmental Science, University of Arizona, Tucson, AZ 85721*

**ABSTRACT:** The goal of this study was to determine effects of temperature and soil type on survival of *Ascaris* ova in two biosolid-amended, desert soils. Results of this study suggest that a waiting period of 120 days at average soil temperatures of 25°C or 90 days at 37°C after land application of biosolids on fields to which lettuce is planted would result in annual risks of less than 1:10,000 for *Ascaris* from consumption of lettuce with an ova concentration of 4 ova/g dry solids.

## INTRODUCTION

**A**SCARIS OVA are believed to be enteric pathogens most resistant to inactivation during sludge and wastewater treatment. Not only are *Ascaris* ova more resistant to treatment processes than other pathogens but they are also more resistant than other helminthes [9]. *Ascaris* ova as a result are one of the microbial parameters utilized for classification of Class A biosolids under Part 503 regulations for land application of biosolids in the United States [17]. These guidelines suggest that helminth ova concentrations should be limited to less than one helminth ova/4 g (0.25/g) total solids (TS) in Class A biosolids. However, there are no limits on helminth concentration in Class B biosolids. The World Health Organization (WHO) in 2006 published guidelines on safe use of fecal material and sludge in agriculture and aquaculture utilizing wastewater. These guidelines require helminth ova content should be less than one viable ova per liter in wastewater used for irrigation [18]. Previous studies have shown inactivation of *Ascaris* ova during various wastewater treatment processes is dependent upon temperature, pH, and humidity [9], but most of the published data is qualitative rather than quantitative and focuses on helminth survival in biosolids. This ignores effects of soil on survival of ova. More quantitative data are necessary to fully understand the relationship between environmental conditions and ova survival so that a more accurate estimate of risk can be made for exposure to land application of Class B biosolids.

Quantitative microbial risk assessment (QMRA) is emerging as a useful tool for developing guidelines for human exposure to pathogens [3,5,10]. QMRA has shown its effectiveness in assessing risk of transmission of water and food-borne infections. Best probabilistic estimates have been obtained using epidemiologic data from actual outbreak studies [10]. When applying QMRA, the first step is to define the best distribution model that fits observed infection rates as a function of pathogen exposure dose. The most common models used to estimate probability of infection are the exponential and the Beta-Poisson models. Major sources of uncertainty in QMRA involve hygiene-related behavior and consumption patterns (water or food) for a targeted population and actual pathogen doses under consideration [10].

The goal here was to assess inactivation of ova in two Arizona soils to which biosolids had been applied and use this information to assess risks of *Ascaris* infection from ingestion of contaminated raw vegetables grown on amended soils.

## MATERIALS AND METHODS

### Sample Preparation

Dewatered, mesophilic, anaerobically digested sludge was obtained from Ina Road Wastewater Reclamation Facility (Tucson, AZ). Biosolids contained 7% total solids as determined via moisture content analysis. Sludge was brought to a pH of 7 beforehand by addition of 1 N NaOH. A sandy loam and a clay loam collected from plots within the University of Arizona Campbell Agricultural Center in Tucson, AZ were

\*Author to whom correspondence should be addressed.  
E-mail: gerba@ag.arizona.edu



used. One gram of soil (i.e., either sandy loam or clay loam) was added to 9.0 g of biosolids and one ml of *Ascaris suum* ova (Excelsior Sentinel, Inc., Trumansburg, NY) was added to obtain a concentration of 6,500 ova/ml in a sterile pre-weighed petri dish or 50 ml glass beaker. Average moisture content measured for biosolid-amended soil samples was 93%.

### Experimental Conditions

Sandy loam samples were held either at room temperature (25°C), 37°C, or left exposed to the outdoor environment for thirty days (i.e., microcosm). Clay loam samples were incubated at 37°C for thirty days. All samples demonstrated greater than 90% loss of moisture within 24 hours of incubation regardless of conditions. The microcosms consisted of placement of the soil/ biosolid mixtures (1 g/9 g) in 50 ml glass beakers placed 2.4 cm below soil surface in a 30 × 20 × 12.5 cm plastic container. Triplicate samples were processed at time intervals of 0 (control), 1, 5, 10, 20, and 30 days. Weather data (temperature and precipitation) were collected from Tucson International Airport located next to the test site for the duration of the experiment.

### Enumeration of *A. suum* Ova within Biosolid-Amended Soil

Samples of soil/biosolid mixtures were weighed and subsequently processed according to a modified Wisconsin flotation method described previously [1]. Samples were suspended in deionized water in 50 ml conical tubes for 30 min and then centrifuged (Beckman CS-6, Beckman Coulter, Indianapolis, IN) for 5 min at 3200 rpm. The resulting supernatant was poured off and this process was repeated 2 to 3 times until the supernatant was clear. Sheather's sucrose solution (specific gravity = 1.27) [1] was added to the biosolid/soil pellet and mixed by vortexing. Additional Sheather's sucrose solution (≈ 35 ml) was added to the sugar biosolid mixture and tubes were then spun at 3200 rpm in a swinging bucket rotor for 15 minutes (Beckman CS-6, Beckman Coulter, Indianapolis, IN). The upper portion of the mixture containing Sheather's sucrose solution (microscopic debris and *Ascaris* ova) was poured into two nested sieves (Erie Scientific, Portsmouth, NH) (63 μm and 38 μm, respectively). Sieves were rinsed with deionized water and contents on the 38 μm sieve were rinsed into a 15 ml conical tube. The 15 ml conical tubes were filled with water and spun

at 3,200 rpm (Beckman CS-6, Beckman Coulter, Indianapolis, IN) for 5 minutes. Resulting supernatant was aspirated off down to 1, 2, or 3 ml and 0.1 to 0.3 ml of ovum solution was mixed with an equal volume of 0.2 N H<sub>2</sub>SO<sub>4</sub>, serially diluted, and placed in a 24-well culture plate. Ova were incubated in the 24-well culture plates at room temperature and examined for viability (development) after 12, 15, and 30 days. Ova were enumerated and examined for viability by scanning each well under light microscopy. Each well was examined for viable ova, non-viable ova, and total ova. For each count, ova were multiplied by an appropriate serial dilution factor to determine amount of viable and non-viable ova contained in the original sample.

### Risk Assessment

A dose-response function has been developed for *Ascaris lumbricoides* based on outbreak data and epidemiological studies [11]. The dose-response relationship developed for *A. lumbricoides* infection consists of a Beta-Poisson model with  $\alpha = 0.104$  in the equation:

$$P(d) = 1 - [1 + (d/N_{50})(2^{1/\alpha} - 1)]^{-\alpha} \quad (1)$$

where  $d$  = estimated dose of *A. lumbricoides* ova and alpha parameters were derive from use of a beta distribution to model non-constant pathogen survival probabilities. This relationship was the end result of fitting observed infectivity and exposure dose estimated for the Mezquital Valley in Mexico [10,11]. Estimated annual risk is given by

$$P_{\text{annual}} = 1 - [1 + P(d)]^n \quad (2)$$

where  $P_{\text{annual}}$  = annual risk of infection in an individual from  $n$  exposures per year to pathogen dose;  $d$  is the total number of organisms in a known consumed amount of either vegetables or soil, based on *A. lumbricoides* concentration for each exposure scenario; and  $N_{50}$  is median infective dose [10].

The following assumptions or scenarios were also used in estimating probability of an *A. lumbricoides* infection from eating raw lettuce grown on biosolid amended soil:

- *A. suum* inactivation in desert soils was calculated from the present study.
- Use of three different helminth concentrations in biosolids (0.25, 1, and 4 per g) based on content found in the United States [10,13].

- An *Ascaris* concentration of 0.0065, 0.0257, and 0.0959 ova/g lettuce based on 0.25, 2, and 4 ova g total solids and a 10% transfer of ova to lettuce leaves at these rates [4].
- A mean intake range estimate of 30, 54, or 100 g per serving of lettuce. Uncooked lettuce was consumed once a week.
- A one log<sub>10</sub> [18] *A. lumbricoides* reduction due to crop washing was assumed to occur in addition to ova inactivation within biosolid amended soil (data from this study). QMRA was conducted 30 and 60 days after biosolid application in addition to the 60 day period necessary for lettuce cultivation [8].

### Statistical Analysis

Statistical significance was assessed via a two-way ANOVA with Tukey's posthoc test ( $\alpha = 0.05$ ) using SigmaPlot software (San Jose, CA). Linear regression values were also obtained using SigmaPlot software.

### RESULTS

Outdoor conditions were measured. Temperature maximum and minimum and rainfall data for samples exposed to the outdoor environment may be found in Table 1.

Temperature varied throughout the month of April during the experiment with a maximum of 34.4°C and a minimum of 2.8°C. Only one rainfall event occurred (day 9) producing 0.28 inches of rain.

Minimum temperature occurred on day 9 of the experiment (14°C). Maximum temperature occurred on days 1 and 2 (34°C). Mean temperature for the duration of the experiment was 21°C. The median minimum and maximum temperature were calculated to be 14°C and 29°C, respectively. Only one rainfall event occurred during the experiment. This event resulted in 7 mm of rain and occurred on day 9 of the experiment.

### Soil Effects on *Ascaris* Viability

Significant differences in log<sub>10</sub> reduction were observed between sandy loam and clay loam soils at 37°C on days 10 and 30 (See Figure 1). Inactivation rates were determined by the slope of a best fit line and linear regression. Inactivation was faster in sandy loam. The r<sup>2</sup> values (obtained from best fit line, SigmaPlot) were 0.972 and 0.998 for sandy loam and clay loam soils, respectively.

**Table 1. Weather Data During Biosolid Amended Sandy Loam Incubation Under Outdoor Conditions.**

Day	Air Temperature (°C)		Precipitation (mm)
	Maximum	Minimum	
1	34.4	15.0	0.0
2	34.4	16.7	0.0
3	29.4	18.33	0.0
4	27.8	12.2	0.0
5	32.8	10.6	0.0
6	28.9	16.7	0.0
7	26.1	15.0	0.0
8	25.0	13.3	0.0
9	13.9	5.0	7.0
10	15.0	2.8	0.0
11	28.9	3.9	0.0
12	27.8	10.6	0.0
13	27.2	10.6	0.0
14	23.3	11.7	0.0
15	30.0	8.9	0.0
16	32.8	10.6	0.0
17	33.9	15.0	0.0
18	32.2	15.6	0.0
19	31.1	17.2	0.0
20	31.7	13.3	0.0
21	30.6	14.4	0.0
22	31.1	15.0	0.0
23	31.1	12.8	0.0
24	28.8	16.1	0.0
25	27.2	14.4	0.0
26	28.3	15.0	0.0
27	28.3	12.7	0.0
28	33.3	12.2	0.0
29	33.3	15.0	0.0
30	26.1	15.0	0.0

### Temperature Effects on *Ascaris* Viability

Significant differences in log<sub>10</sub> reductions were observed in sandy loam incubated at either 37°C or 25°C when compared to the outdoor ambient temperatures study (mean 21°C), after 10 and 30 days (See Figure 2). However, after 20 days log<sub>10</sub> reduction at 25°C and ambient outdoor temperature were similar but significantly different than at 37°C. Inactivation rates for 25°C and outdoor ambient incubation were similar while 37°C showed maximum inactivation rate. The r<sup>2</sup> values were 0.972, 0.980, and 0.987 for incubations in

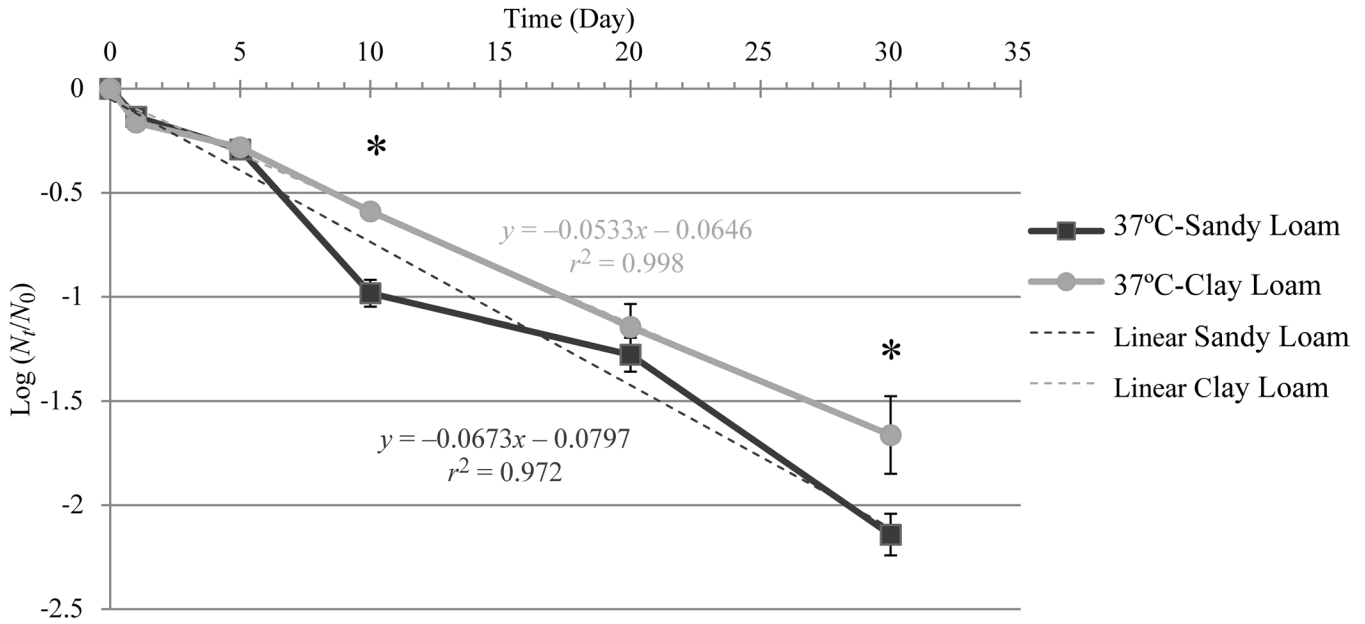


Figure 1. Effect of soil type on *Ascaris* survival at 37°C.

the sandy loam soil at temperatures of 37°C, 25°C, and for the outdoor ambient study, respectively.

**QMRA of Ingesting Raw Vegetables Grown in Biosolid-Amended Soil**

Scenario 1, annual risk of *Ascaris* infection from ingesting raw lettuce grown on biosolid amended sandy loam assuming a soil temperature of 37°C. Table 2 displays how temperature effects risk of infection over time. All annual risks for this scenario are less than 1:10,000 even at the highest *Ascaris* concentration (4

ova/g TS) and lettuce consumption rate (100 g/d) examined.

The log inactivation for these calculations represents the log inactivation obtained from experimentation plus 1 log<sub>10</sub> for loss during washing (Total log removal due to inactivation and loss after crop washing).

Scenario 2, annual risk of *Ascaris* infection from ingesting raw lettuce grown on biosolid amended sandy loam assuming a soil temperature of 25°C. Table 3 displays how duration of time between biosolid applications and consumption of lettuce under these conditions impacts annual risk. *Ascaris* concentrations at or

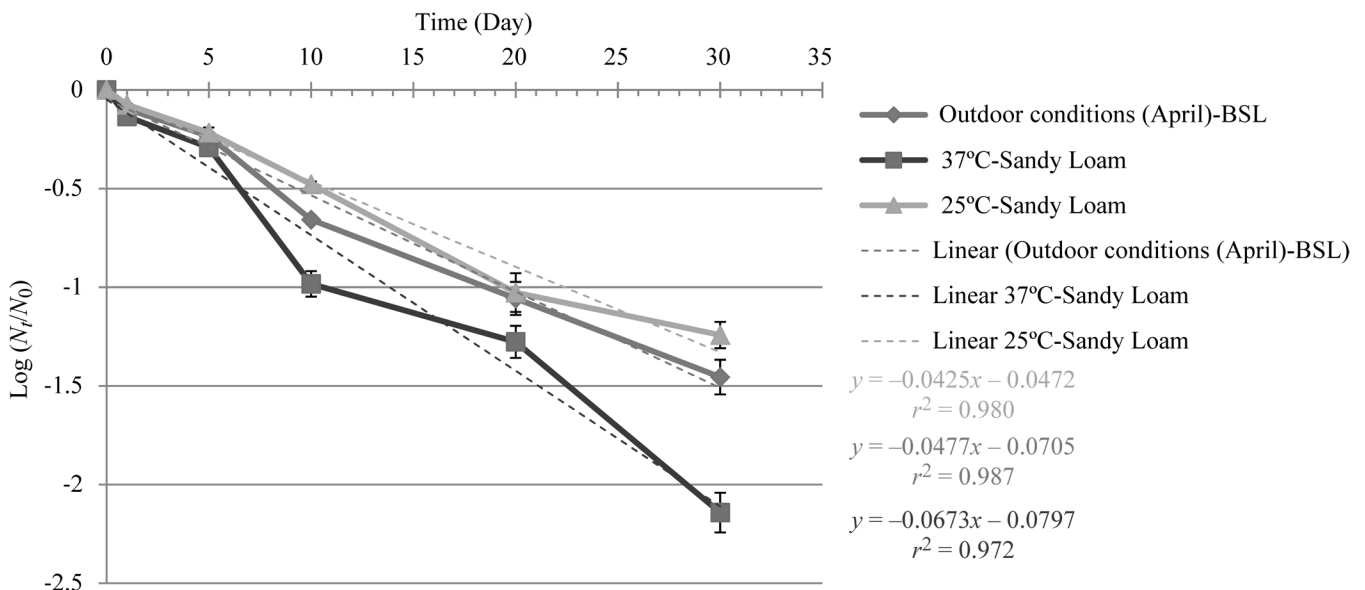


Figure 2. Effect of temperature on *Ascaris* survival in sandy loam soil.

**Table 2. Annual Risk of Infection from *Ascaris ova* After Various Harvesting Times in Biosolid Amended Sandy Loam at 37°C.**

Scenarios			Annual Risk	
Biosolids (ova/g TS)	Lettuce (ova/g)	Lettuce Consumption (g/d)	90 Days Post-application	120 Days Post-application
0.25	0.0065	30	8.3E-08	8.7E-10
0.25	0.0065	65	1.8E-07	1.8E-09
0.25	0.0065	100	2.8E-07	2.7E-09
1	0.0257	30	3.3E-07	3.2E-09
1	0.0257	65	7.1E-07	6.9E-09
1	0.0257	100	1.1E-06	1.1E-08
4	0.0959	30	1.2E-06	1.2E-08
4	0.0959	65	2.6E-06	2.6E-08
4	0.0959	100	4.1E-06	4.0E-08

above 1 ova/g TS in conjunction with lettuce consumption rates at or above 65 g/d resulted in risks greater than 1:10,000 when the post-application period was 90 days. Calculated risk of infection was less than 1:10,000 for this scenario at 120 days post-application.

The log reduction represents the log inactivation obtained from experimentation plus 1 log<sub>10</sub> for loss during washing (Total log removal due to inactivation and loss after crop washing).

Scenario 3, annual risk of *Ascaris* infection from ingesting lettuce grown on biosolid amended sandy loam assuming an outdoor ambient soil temperature (mean 21°C). Table 4 also displays that duration of time under these conditions impacts annual risk. Risk of infection for 90 days post-application was greater than 1:10,000 at *Ascaris* concentrations of 4 ova/g TS and consump-

tion rates of at least 65 g/d. However, risk of infection was less than 1: 10,000 for any assumption at 120 days post-application.

The log reductions represent the log inactivation obtained from experimentation plus 1 log<sub>10</sub> for loss during washing (Total log removal due to inactivation and loss after crop washing)

## DISCUSSION

### *Ascaris* Survival in Biosolid Amended Soils

Soil type was shown to play a role in the survival of *A. suum* ova (See Figure 1). Ova incubated in biosolid amended clay loam had a lower inactivation rate than ova incubated in the biosolid amended sandy loam.

**Table 3. Annual Risk of infection from *Ascaris ova* After Various Harvesting Times in Biosolid Amended Sandy Loam at 25°C.**

Assumptions			Annual Risk	
Biosolids (ova/g TS)	Lettuce (ova/g)	Lettuce Consumption (g/d)	90 Days Post-application	120 Days Post-application
0.25	0.0065	30	1.3E-05	8.2E-07
0.25	0.0065	65	2.7E-05	1.8E-06
0.25	0.0065	100	4.2E-05	2.7E-06
1	0.0257	30	4.9E-05	3.2E-06
1	0.0257	65	1.1E-04	7.0E-06
1	0.0257	100	1.6E-04	1.1E-05
4	0.0959	30	1.8E-04	1.2E-05
4	0.0959	65	4.0E-04	2.6E-05
4	0.0959	100	6.1E-04	4.0E-05

**Table 4. Annual Risk of Infection from *Ascaris ova* After Various Harvesting Times in Biosolid Amended Sandy Loam Under Outdoor Conditions.**

Assumptions			Annual Risk	
Biosolids (ova/g TS)	Lettuce (ova/g)	Lettuce Consumption (g/d)	90 Days Post-application	120 Days Post-application
0.25	0.0065	30	6.2E-06	2.0E-07
0.25	0.0065	65	1.3E-05	4.4E-07
0.25	0.0065	100	2.1E-05	6.7E-07
1	0.0257	30	2.4E-05	8.0E-07
1	0.0257	65	5.3E-05	1.7E-06
1	0.0257	100	8.1E-05	2.7E-06
4	0.0959	30	9.1E-05	3.0E-06
4	0.0959	65	2.0E-04	6.5E-06
4	0.0959	100	3.0E-04	9.9E-06

Clay and silt particles retain moisture very efficiently and, therefore pathogens introduced into a soil with moderate or high clay and/or silt content shows enhanced survival [12]. When incubated at temperatures between 20°C and 38°C, survival times for *Ascaris ova* have been shown to be less than 90 days in sandy soil and greater than 90 days in soils with higher clay content [2].

Soil temperature was also found to play a role in the survival of *A. suum* ova (See Figure 2). Ova incubated at 25°C in biosolid amended sandy loam showed lower inactivation rates than those incubated outdoors. Ova incubated at 37°C had the highest inactivation. Similar results have been reported in other studies [9] and show that higher temperatures significantly affect survival of *Ascaris ova*. *Ascaris ova* have been shown to survive for up to one year in biosolids held at temperatures between 17°C and 20°C [16]. Johnson *et al.* (1998) [6] found a 95% inactivation of *Ascaris ova* in five weeks when incubated at 35°C in sludge. Studies have shown that temperatures above 40°C result in *Ascaris* inactivation in only two days [7]. Temperatures above 50°C have been shown to result in *Ascaris* inactivation in as little as 2 hours [15,7].

### Risk Assessment

Infectious risks from helminth ova are dependent on ova concentrations in biosolids, lettuce consumption, and *Ascaris* ovum inactivation. It is important to note that duration of time between biosolids application and harvest includes the period of time necessary for the growth of lettuce. It takes 30 to 60 days for lettuce to

be harvest-ready after planting. With a one log<sub>10</sub> reduction due to crop washing risk of infection ranged from a low of 8.1E-10 at a helminth ovum concentration of 0.25 g TS in biosolids to a high of 6.1E-04 at a helminth ovum concentration of 4 g TS in biosolids. Risk of infection may be underestimated by using lower than actual transfer rates of *Ascaris* to lettuce and also by underestimating lettuce consumption. Conversely, risk of infection may be overestimated by overestimating transfer rates of *Ascaris* to lettuce and lettuce consumption.

Lowest risk resulted from the scenario of eating raw lettuce grown on biosolid amended sandy loam soil which was incubated at 37°C (See Table 2). This is due to *Ascaris* ovum inactivation being greatest under these conditions. The greatest risk resulted from eating raw lettuce grown on biosolid amended sandy loam incubated at 25°C (See Table 3). *Ascaris* ovum inactivation under these conditions was at a minimum yielding a greater risk. The United States Environmental Protection Agency has used a 1:10,000 yearly risk of infection as guidance for treatment of surface water intended for drinking [14]. Currently the U. S. EPA requires up to two years before food crops can be grow on land to which Class B biosolids have been applied [17]. Results of this study suggest that a waiting period of 120 days at 25°C or 90 days at 37°C after land application of biosolids on fields to which lettuce is planted would result in yearly risks of less than 1:10,000 for *Ascaris* from consumption of the lettuce if ova concentration in the biosolids was 4 ova g dry solids. With reported ova concentration generally less than 0.25 ova g TS in Class B biosolids in the United States [13] a consider-

able margin of safety exists from land application of Class B biosolids and risk from *Ascaris* infection from production of food crops eaten raw in desert regions.

## ACKNOWLEDGEMENTS

This study was funded in part by the National Science Foundation Water and Environmental Technology (WET) Center located at the University of Arizona.

## REFERENCES

1. Cox, D.D. and Todd, A.C. (1962). Survey of gastrointestinal parasitism in Wisconsin dairy cattle, *Journal of the American Veterinary Medical Association*, Vol. 141, No.6, pp. 706–709.
2. Feachem, R.G. (1980) *Appropriate Technology for Water Supply and Sanitation: Health Aspects of Excreta and Sullage Management*. Washington, DC: Energy, Water and Telecommunications Department of the World Bank.
3. Haas, C.N., J. B. Rose and C.P. Gerba (2002) Progress and data gaps in quantitative microbial risk assessment, *Water Science Technology*, Vol. 46, No. 11-12, pp. 277–284.
4. Jimenez, B., S. Austin, E. Cloete and C. Phasha (2006) Using Ecosan sludge for crop production, *Water Science and Technology*, Vol. 54, No. 5, pp. 169–177.
5. Jimenez, B. (2007) Helminth ova control in sludge: a review. *Water Science and Technology*, Vol. 56, No. 9, pp. 147–155.
6. Johnson, P.W., R. Dixon and S. D. Ross (1998) An in-vitro assessing the viability of *Ascaris suum* eggs exposed to various sewage treatment processes, *International Journal of Parasitology*, Vol. 28, No. 4, pp. 627–633.
7. Kato, S., E., Fogarty and D. D. Bowman (2003) Effect of aerobic and anaerobic digestion on the viability of *Cryptosporidium parvum* oocysts and *Ascaris suum* eggs, *International Journal of Environmental Health Research*, Vol. 13, No. 2, pp. 169–179.
8. Kerns, D.L. (1999) *Guidelines for Head Lettuce Production in Arizona*. IPM series number 12. Publication number az1099. University of Arizona, Tucson.
9. Maya, C., M. Ortiz and B. Jimenez (2010) Viability of *Ascaris* and other helminth genera non larval eggs in different conditions of temperature, lime (pH) and humidity, *Water Science Technology*, Vol. 62, No. 11, pp. 2616–2624.
10. Navarro, I., B. Jimenez, E. Cifuentes and S. Lucario (2009) Application of Helminth ova infection dose curve to estimate the risks associated with biosolid application on soil, *Journal of Water Health*, Vol. 7, No. 1, pp. 31–44.
11. Navarro, I. and B. Jimenez, (2011) Evaluation of the WHO helminth eggs criteria using a QMRA approach for the safe reuse of wastewater and sludge in developing countries, *Water Science Technology*, Vol. 63, No. 7, pp. 1499–1505.
12. Pepper, I.L., M. Brusseau and C. P. Gerba (2006) *Environmental Pollution Science*. Boston, MA: Elsevier/Academic Press.
13. Pepper, I.L., J. P. Brooks, R. G. Sinclair, P. L. Gurian and C. P. Gerba. (2010) Pathogens and indicators in United States Class B biosolids: national and historic distributions, *Journal of Environment Quality*, Vol. 39, No. 1, pp. 2185–2190.
14. Regli, S., J. B. Rose, C. H. Haas, and C. P. Gerba. 1991. Modeling the risk from *Giardia* and viruses in drinking water, *Journal of the American Water Works Association*, Vol. 83, No. 11, pp. 76–84.
15. Schmidt, G.D. and L.S. Roberts. (1981) *Foundations of Parasitology*. Maryland Heights, MO: Mosby Company.
16. Strauss, M. and Blumenthal, U. J. (1990) *Human Waste in Agriculture and Aquaculture: Utilization Practices and Health Perspectives*. Duedendorf, Germany: International Reference Centre for Waste Disposal. (IRCWD Report No. 09/90).
17. US EPA (1993). *Standards for the use and Disposal of Sewage Sludge*. Washington, DC: EPA 822/Z-93/001.
18. WHO (2006) *Guidelines for the Safe Use of Wastewater, Excreta and Greywater*. Geneva, Switzerland: World Health Organization.



# Removal of a Reactive Dye using Ash of Pulp and Paper Sludge

A. AZIZI<sup>1</sup>, M.R. ALAVI MOGHADDAM<sup>2,\*</sup> and M. ARAMI<sup>3</sup>

<sup>1</sup>PhD. student of Civil and Environmental Engineering, Department of Civil and Environmental Engineering, Amirkabir University of Technology (AUT), Hafez Ave., Tehran15875-4413, Iran

<sup>2</sup>Associate professor, Department of Civil and Environmental Engineering, Amirkabir University of Technology (AUT), Hafez Ave., Tehran15875-4413, Iran

<sup>3</sup>Professor, Department of Textile Engineering, Amirkabir University of Technology (AUT), Hafez Ave., Tehran15875-4413, Iran

**ABSTRACT:** The aim of this study was to examine performance of pulp and paper sludge ash of Mazandaran wood and paper industries for removal of reactive blue 19 dye. Maximum dye removal efficiency (95%) occurred at a pH of 12. Maximum dye adsorption with increasing adsorbent dose reached 92.59% at 12 g/L of adsorbent dose. Q increased with an increasing of initial dye concentration and reached a maximum value of 85.81 mg dye/g adsorbent. The adsorption process follows a Temkin isotherm model and the Elovich order kinetic model. The dye removal efficiency was obtained 59.16% for actual textile wastewater.

## INTRODUCTION

**T**HE majority of dyes are synthetic in nature and are difficult to decolorize due to their complex structure. Most dyes contain aromatic rings which make them mutagenic and carcinogenic [1]. Many methods are reported to remove dyes from effluents and technologies may be divided into three categories including biological, chemical, and physical methods [2,3].

Among various available technologies the adsorption process is valuable because of convenience, ease of operation, and simplicity of design [4]. Recently, some investigations have reported using non-conventional low-cost adsorbents including natural materials and waste materials from industry and agriculture for dye removal such as acid-treated pine cone powder [5], coconut husk [6], coal combustion ashes [7], modified wheat straw [8], metal hydroxide sludge [9], and sewage sludge [10].

Rapidly increasing environmental contamination arising from industrial processes via solid residuals is an important environmental problem requiring attention. Management of pulp and paper industries wastes (e.g., wood waste, pulp, and paper sludge) in recent years also has become a significant environmental issue. Because of its large daily output and limited landfill space some investigations have proposed different

applications for uses of sludge such as soil improvers, fertilizers, and building materials [11]. Previously, performance of wood waste [12] and dried and treated pulp and paper sludge [13,14] on reactive blue 19 dye adsorption was tested using classical and statistical [15,16] methods. Also, some of these industries implemented sludge incineration systems to reduce residual amounts in order to solve the problem of insufficient landfill sites. Therefore, reuse of this residual (pulp and paper sludge ash) has been considered.

The aim is to evaluate potential of pulp and paper sludge ash (PPSA) as another alternative adsorbent for removal of reactive dye (RB19). Effect of contact time, pH, adsorbent dose, and initial dye concentration on performance of the adsorption process were studied. Langmuir, Freundlich, and Temkin isotherms were used to describe adsorption isotherms. In addition, the pseudo-first order, the pseudo-second order, and Elovich models were studied to describe adsorption kinetics. Furthermore, treatment of real textile wastewater was also examined.

## MATERIALS AND METHODS

### Preparation of Synthetic and Real Textile Wastewater

Reactive blue 19 (Ariazol Brill. Blue R-SP) was provided by the Alvan Sabet Company in Iran and is used for preparation of synthetic wastewater. General

\*Author to whom correspondence should be addressed.  
E-mail: alavi@aut.ac.ir, alavim@yahoo.com



properties and chemical structure are presented in Table 1. This dye is widely used in textile industries in Iran. A stock dye solution of 1000 mg/L was prepared in double distilled water and then diluted to obtain a desired concentration. Solution pH was adjusted with HCl and NaOH and pH measurement was carried out using a 340i/SET pH meter (WTW-Germany).

Also, real textile wastewater containing reactive blue 19 dye was collected from the Negin-Nakhe-Beshel Company, in Mazandaran, North of Iran. This real wastewater has some additives including NaCl,  $\text{Na}_2\text{CO}_3$ , caustic NaOH, cationic ion exchange, detergent (ABS), cationic softener, antifoam, and other chemical agents. Characteristics of the real textile wastewater are as follows: RB19 concentration = 500 mg/L, pH = 10, COD (chemical oxygen demand) = 1000 mg/L, and NTU (nephelometric turbidity unit) = 7.94.

### Preparation of Adsorbent

Pulp and paper sludge used in this study was collected from Mazandaran wood and from the paper industries (MWPI) in Mazandaran, Iran. This factory is the largest paper manufacture in Iran and produces 100–120 tones of air dried sludge daily. Collected sludge was dried at room temperature in a laboratory for 48 hours. Pulp and paper sludge was grounded and sieved by 150  $\mu\text{m}$  sieve. Sludge particles less than 150  $\mu\text{m}$  sieve were heated in an oven at 550°C for 3 hours. Then, pulp and paper sludge ash was stored in an air-tight glass container and used as adsorbent.

As determined by XRF using a X<sup>3</sup>Uniqe model XRF analyzer (Philips, Netherlands), chemical composition of pulp and paper sludge was 9.7%  $\text{Al}_2\text{O}_3$ , 0.27%  $\text{Fe}_2\text{O}_3$ , 16.4% CaO, 1.46% MgO, 3.8%  $\text{SiO}_2$ ,

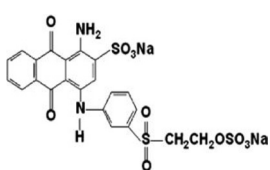
3.52%  $\text{SO}_3$ , 0.11%  $\text{Na}_2\text{O}$ , 0.12%  $\text{K}_2\text{O}$ , and 0.2%  $\text{P}_2\text{O}_5$ . Loss on ignition (LOI) of pulp and paper sludge was found to be 64.25% by weight. Other trace elements analyzed were not reported due to very small quantity. A scanning electron microscope (SEM) was used to characterize the PPSA sample for morphological information using a XL-C model SEM analyzer (Philips, Netherlands). Textural properties of adsorbent were also carried out by  $\text{N}_2$  adsorption/desorption isotherms at 77K using an Autosorb 1 analyzer (Quantachrome Corporation, USA). Specific surface area ( $S_{\text{BET}}$ ) was calculated using the Brunauer–Emmett–Teller (BET) method. Pore size distribution was determined using the Barrett–Joyner–Halenda (BJH) method.

Instructions from Ahmad and Kumar [17] were used for determination of point of zero charge of PPSA. Next, 0.1 M KCl was prepared and its initial pH was adjusted between 2 and 12 using NaOH and HCl. Then, 50 ml of 0.1 M KCl was taken in 250 ml beakers and 0.05 g of PPSA was added to each solution. These beakers were kept for 24 hours and the final pH of solutions was measured using a pH meter. Graphs were plotted between  $\text{pH}_{\text{final}}$  and  $\text{pH}_{\text{initial}}$  and the pH of zero point charge of PPSA is about 8.6 as displayed in Figure 1.

### Batch Adsorption Experiments

Dye solution and adsorbent were agitated using a jar test at 150 rpm agitation speed. A six beakers jar test apparatus from Zag-Chemi Company in Iran was used to simulate the adsorption process. Prior to the analysis all samples were centrifuged at 5,000 rpm for 10 minutes. Dye concentration of synthetic wastewater and the real textile wastewater were measured using a

**Table 1. General Properties and Chemical Structure of RB19.**

Parameters	Values
C. I. name	0.RB19
Empirical formula	$\text{C}_{22}\text{H}_{16}\text{N}_2\text{Na}_2\text{S}_3$
$\lambda_{\text{max}}$ (nm)	594
Molecular weight	626.54
Chemical structure	

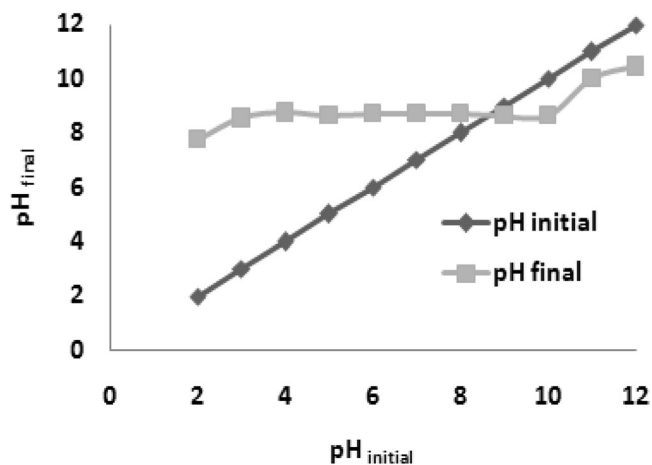


**Figure 1. Point of zero charge of PPSA.**

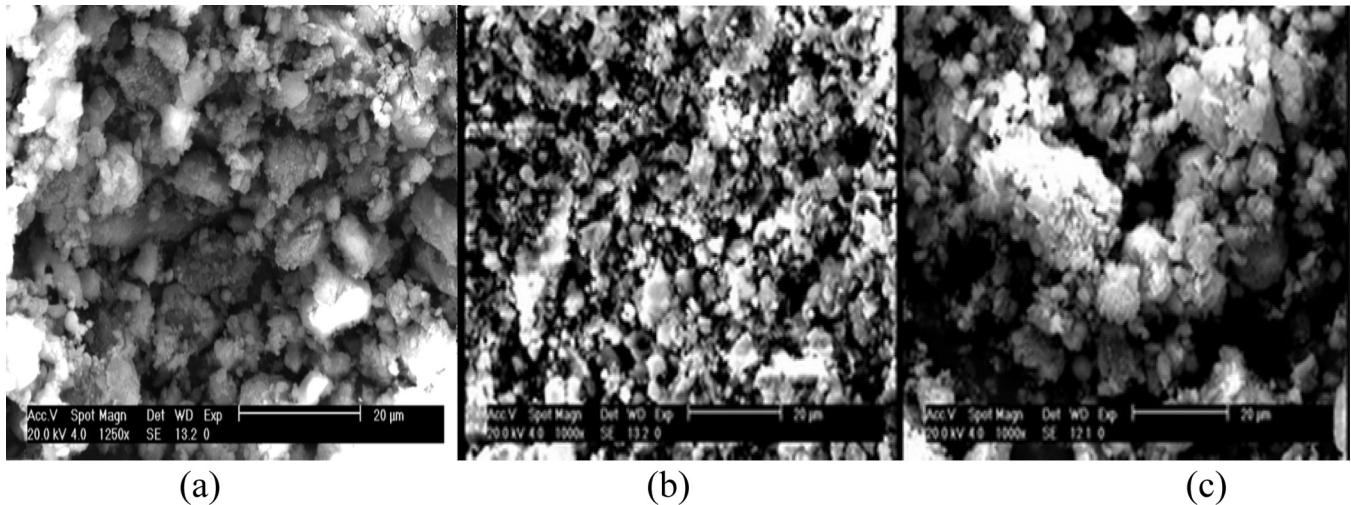


Figure 2. SEM images of (a) dried pulp and paper sludge, (b) PPSA sample before, and (c) after adsorption process.

HACH spectrophotometer DR/4000 (USA). Sorption studies were carried out at  $23 \pm 1^\circ\text{C}$ . Percentage of dye removal was calculated using the following equation:

$$\text{Dye removal (\%)} = \frac{C_0 - C_t}{C_0} \times 100 \quad (1)$$

where,  $C_0$  and  $C_t$  (mg/L) are initial dye concentration and concentration at equilibrium time  $t$  (min), respectively.

## RESULTS AND DISCUSSIONS

### Characterization of Adsorbent

A scanning electron microscope (SEM) is a primary tool for characterizing surface morphology and fundamental physical properties of the adsorbent. SEM pictures (See Figure 2) display morphology of dried pulp and paper sludge (PPSA samples before and after the adsorption process). It is clear that dried pulp and paper sludge after ash obtained more numbers of pores as well as higher surface area. Also, SEM pictures display a porous adsorbent morphology with pores of different sizes and shapes where there is a good possibility for dye to be trapped and adsorbed into these pores.

For textural characteristics of PPSA, BET surface area of  $48.8 \text{ m}^2/\text{g}$  (computed in the  $P/P_0$  range 0.05–0.30), pore volume of  $0.2312 \text{ cm}^3/\text{g}$ , and a pore diameter of  $22.29 \text{ \AA}$  were obtained. Surface areas of other adsorbents were compared in Table 2. Displayed in Table 2 BET surface area of PPSA was higher than BET surface area of dried pulp and paper sludge from

the current authors previous study ( $16.22 \text{ m}^2/\text{g}$ ) [15]. Therefore, according to Figure 2 and Table 2, textural and surface area for PPSA became smaller and higher, respectively. Better adsorption capacity certainly would be expected following this finding.

Also, pore size distribution of the adsorbent is displayed in Figure 3. Generally, pores are divided into micropores ( $< 2 \text{ nm}$ ), mesopores ( $2\text{--}50 \text{ nm}$ ), and macropores ( $> 50 \text{ nm}$ ) [18]. Displayed in Figure 3 the percentages of mesopore and macropores volume of PSSA are higher than for micropore volume.

### Effect of Contact Time on Dye Adsorption

Effect of contact time on RB19 adsorption efficiency is presented in Figure 4. Experiments for this step were done with a constant initial concentration of  $100 \text{ mg/L}$ , PPSA dose of  $4 \text{ g/L}$ , and at pH of 11. Adsorption efficiency increases with increasing contact time.

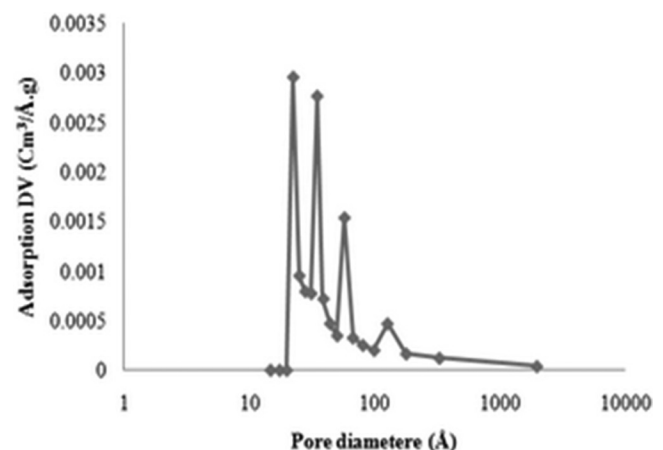


Figure 3. Pore size distribution of PPSA.

**Table 2. Surface of Area of Adsorbents.**

Adsorbent	Surface Area (m <sup>2</sup> /g)	References
pistachio hull waste	1.04	[19]
Dried pulp and paper sludge	16.22	[15]
Coal combustion ashes	19	[7]
Paper sludge heated 600	23	[11]
PPSA	48.8	Present study
Cocoa (Theobroma cacao) shell-based activated carbon	85.09	[20]
Bone char	107	[18]
Activated carbon from Bagasse pith (using H <sub>3</sub> PO <sub>4</sub> )	522.7	[21]
Activated carbon from Typha orientalis (using KMnO <sub>4</sub> )	556.49	[22]
Commercial activated carbon, F400	793	[18]
Activated carbon from bamboo	1400	[18]

Very rapid adsorption is observed in the first minutes and thereafter rate of adsorption was found to be slow and then constant. A similar result was presented by the current research group [12–14] as well as by other researchers for investigating contact time effect on using activated carbon and from orange peel for Direct N Blue-106 [23] and direct blue 86 [24] dye removal and crystal violet dye removal using phase change material [25] during the adsorption process. It was discovered that 90.18% removal of RB19 occurred at 30 minutes and after that no significant change was observed. Regarding results here, 30 minutes of contact time was selected for further experiments for the adsorption process.

### Effect of pH on Dye Adsorption

pH is one of the important factors influencing ad-

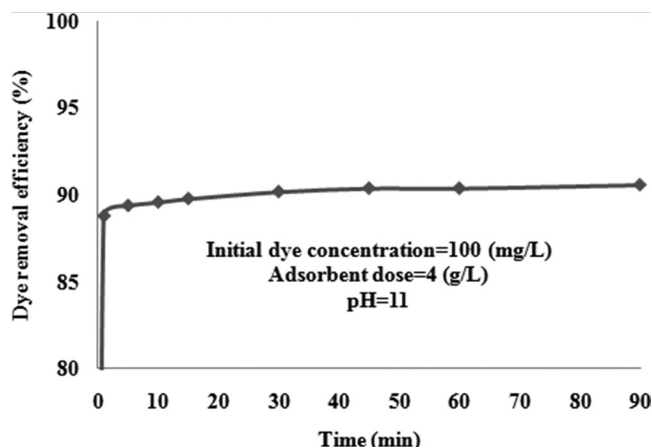


**Figure 4.** Effect of contact time on RB19 adsorption by PPSA (adsorbent dose = 4 g/L; initial dye concentration = 100 mg/L; and pH = 11).

sorption efficiency. Experiments during this stage were performed with a constant initial concentration of 100 mg/L, adsorbent dose of 4 g/L, and contact time of 30 minutes. Results are illustrated in Figure 5 and high removal efficiency occurred for both acidic and alkaline conditions. A similar result was observed by other researchers for removal of different types of dyes [26,27]. Different mechanisms may be used to interpret this phenomenon.

The pH of zero point charge of PPSA is about 8.6. Surface charge of PPSA is neutral at  $pH_{zpc}$ . Below the  $pH_{zpc}$ , adsorbent surface is positively charged and above the  $pH_{zpc}$  adsorbent surface is negatively charged [28]. Maximum observed adsorption capacity at low pH may be due to electrostatic attractions between negatively charged  $-SO_3^-$  groups in the dye molecule and the positively charged adsorbent's sur-

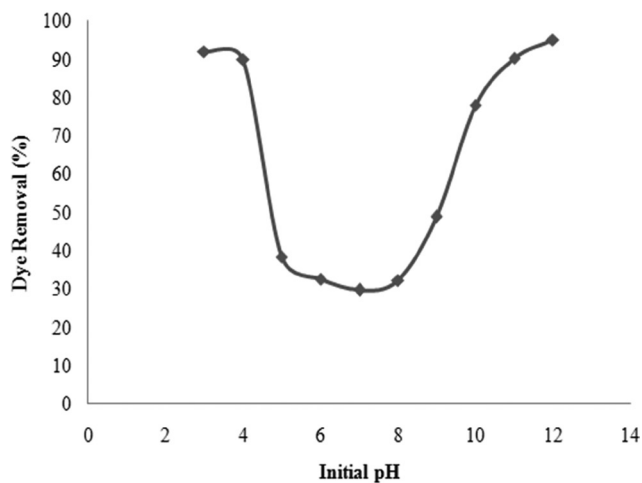


**Figure 5.** Effect of pH on removal of RB19 dye by PPSA (adsorbent dose = 4 g/L; initial dye concentration = 100 mg/L; and contact time = 30 min).

face [29]. A proportional decrease in adsorption can take place as pH of the solution increased due to electrostatic repulsion between negatively charged sites on the adsorbent and dye anions. There was also competition between  $\text{OH}^-$  at high pH and dye anions for positively charged adsorption sites [23,28]. Yet, higher adsorption of alkaline pH may be due to a different mechanism which may be the reaction of  $\text{Ca}^{2+}$  with anionic dye molecules [27]. This mechanism was related to presence of high calcium derived from calcium oxide as a major component of the adsorbent. Calcium oxide was in contact with water, the hydration reaction occurred, and calcium hydroxide reformed. Partially dissolved  $\text{Ca}(\text{OH})_2$  results in dissociation of  $\text{Ca}^{2+}$  and  $\text{OH}^-$  ions. Exchange sites and dissociation of  $\text{CaO}$  of PPSA may generate  $\text{Ca}^{2+}$  ions. Presence of  $\text{Ca}^{2+}$  in solution and formation of Ca-anionic dye molecules precipitation through the reaction resulted in dye removal [27]. During a high pH the removal reaction would be dominated by chemical precipitation as discussed in the aforementioned.

High removal efficiency of 92% and 95% was obtained at pH 3 and pH 12, respectively. Additionally, effectiveness of different pH (2–12) on stability and dye adsorption of RB19 was investigated. It was observed RB19 dye is quite stable in this range of pH. A similar result was reported by Mahmoud *et al.* 2007 for RB 19 dye [30]. Therefore, observed dye removal is only the result of the adsorption process. Initial pH of solution without changing pH was about 10.7. Due to less consumption of chemicals optimum pH was selected as pH 11.

### Effect of PPSA Dose on Dye Adsorption

During this stage various amounts of adsorbent ranging from 0.5 to 12 g/L were studied under the following conditions: initial dye concentration of 100 mg/L, contact time of 30 minutes, and a pH of 11. The effect of adsorbent dose on RB19 adsorption efficiency is displayed in Figure 6. Percentage of dye removal increased with increasing PPSA amount. This is due to increases in adsorbent sites for adsorption of dye with increased adsorbent dosage [31]. Similar results have been reported by our research group [12–14] as well as others for adsorption of other dyes [31–33]. Minimum and maximum removal efficiency was obtained at 53% and 92.59% at a PPSA dose of 0.5 g/L and 12 g/L, respectively. For this study, a 4 g/L PPSA dose was chosen as optimum adsorbent concentration.

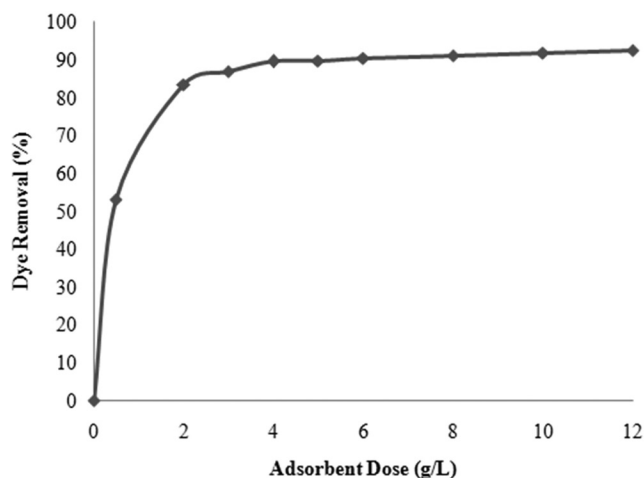


**Figure 6.** Effect of adsorbent (PPSA) dose on removal of RB19 dye (pH = 11; initial dye concentration = 100 mg/L; and contact time = 30 min).

### Effect of Initial Dye Concentration on Dye Removal

Behavior of RB19 adsorption efficiency on PPSA was studied under various initial dye concentrations ranging from 25 to 500 mg/L. PPSA dose was kept constant at 4 g/L and pH was adjusted to 11. Results are presented in Figure 7. Removal efficiency increased from 84.84% to 90% with increases of initial dye concentration ranging from 25 mg/L to 100 mg/L and then decreased from 90% to 68.65% for the initial dye concentration between 100 to 500 mg/L. Initial number of dye molecules is low at a lower concentration. However, available surface area of the adsorbent is high [34,35]. Therefore, when increasing initial dye concentration from 25 mg/L to 100 mg/L the dye concentration to adsorbent sites ratio will be higher. A similar trend was also observed by this group for removal of RB 19 using dried pulp and paper sludge [13] and wood waste [12] as well as other from another researcher for removal of acid yellow 17 using brewing industry waste [34].

$Q$  or the amount of removed dye per unit mass of adsorbent (mg/g) versus initial dye concentration is displayed in Figure 7. It was observed that  $Q$  increased with increases of dye concentration and reached from 5.3 to 85.81 mg removed dye/g PPSA. Similar trends were presented by other researchers for dye removal [33,36,37]. For example, modified rice straw [32], activated carbons prepared from sunflower seed hull [38], and orange peel activated carbon [23] exhibited more adsorption capacity. This may be due to special types of activation processes

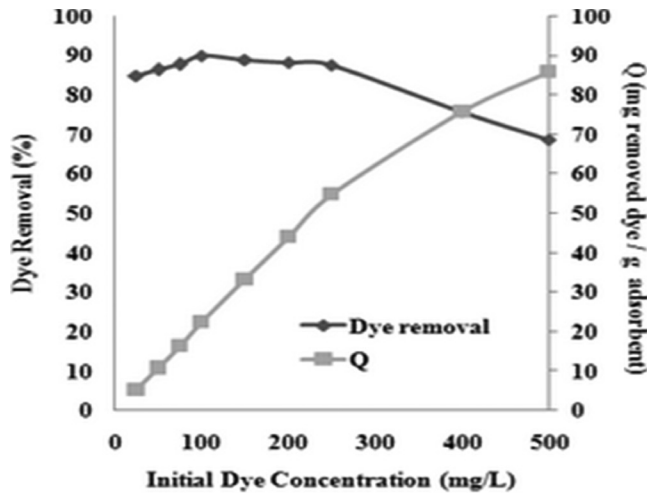


Figure 7. Effect of initial dye concentration on dye removal efficiency and  $Q$  ( $pH = 11$ ; adsorbent dose = 4 g/L; and contact time = 30 min).

on to raw materials which were altered into better adsorbents. However, adsorption capacity of PPSA compared more to adsorption capacity of lignin [39], cotton plants wastes [37], coir pith, sawdust, sugarcane fiber [40], and *Mansonia* wood sawdust [41]. In addition, adsorption capacity of PPSA and other adsorbents derived from MWPI as well as other example adsorbents are displayed in Table 3.

## Adsorption Isotherms

The adsorption isotherm indicates how adsorption molecules distribute between the liquid phase and solid phase when the adsorption process reaches an equilibrium state [20]. An interaction between the adsorbent and adsorbate to obtain adsorption isotherm studies were carried out with different initial dye concentration ranging from 25 to 500 mg/L while adsorbent doses of 4 g/L, contact times of 30 minutes, pH's of 11, and temperatures of  $23 \pm 1^\circ\text{C}$  were kept constant. Three important isotherms the Langmuir, Freundlich, and Temkin were tested. Isotherms parameters are provided in Table 4 [45]. Applicability of the Langmuir isotherm suggests monolayer coverage of the dye on the surface of the adsorbent [46]. The Freundlich isotherm is regarded as an empirical isotherm and indicates surface heterogeneity of the adsorbent [21]. The Temkin isotherm assumes that heat of adsorption for all molecules in the layer decreases linearly with coverage due to adsorbent-adsorbate interactions, and adsorption is characterized by a uniform distribution of binding energies up to some maximum binding energy [47].

A correlation coefficient from three isotherm models and a Chi-square test was used for finding the best isotherm model for adsorption of RB19 on PPSA.

Table 3. Adsorption Capacity of Different Adsorbents.

Adsorbents	Dye	Adsorption Capacity (mg/g)	References
Wood waste (WW)	Reactive blue 19	30.92	[12]
Dried pulp and paper sludge (DPPS)	Reactive blue 19	33.11	[13]
Acid treated pulp and paper sludge (ATPPS)	Reactive blue 19	35.6	[14]
Basic treated pulp and paper sludge (BTPPS)	Reactive blue 19	18.7	[14]
ZnCl <sub>2</sub> treated pulp and paper sludge (ZTPPS)	Reactive blue 19	47.7	[14]
Pulp and paper sludge ash (PPSA)	Reactive blue 19	85.81	present study
Treated ginger waste	Malachite green	84.03	[17]
Orange peel activated Carbon	Direct Nblue_106	107.53	[23]
Lignin	Reactive red HE_3B	10.7	[39]
<i>Mansonia</i> wood sawdust	Methyl violet	24.6	[41]
Modified rice straw	Basic green 4	238.1	[32]
cotton plant wastes	Remazol Black B reactive dye	35.7	[37]
activated carbon prepared from jute sticks	Brilliant Green dye	480	[42]
Lignite	Methylene blue	370	[43]
Magnetic fluid modified peanut husks	Crystal violet	80.9	[44]
activated carbons from sunflower seed hull	Acid blue 15	125	[38]
Coir Pith	Rhodamine B	55.54	[40]
Sawdust	Rhodamine B	17.35	[40]
Sugarcane Fiber	Rhodamine B	15.98	[40]

**Table 4. Isotherm Equations.**

Isotherm Name	Isotherm Equation	Parameters
Langmuir isotherm	$\frac{C_e}{q_e} = \frac{1}{K_L Q_m} + \frac{C_e}{Q_m} \quad (2)$	$C_e$ = concentration of dye at equilibrium (mg/L) $q_e$ = amount of dye adsorbed per amount of adsorbent at equilibrium (mg/g) $K_L$ = Langmuir adsorption constant (L/mg) $Q_m$ = theoretical maximum adsorption capacity (mg/g)
Freundlich isotherm	$\log q_e = \log K_F + \frac{1}{n} \log C_e \quad (3)$	$C_e$ = concentration of dye at equilibrium (mg/L) $q_e$ = amount of dye adsorbed per amount of adsorbent at equilibrium (mg/g) $K_F$ = an indicator of the adsorption capacity (mg/g (L/mg) <sup>1/n</sup> ) $n$ = adsorption intensity
Temkin isotherm	$q_e = B_1 \ln K_T + B_1 \ln C_e \quad (4)$	$C_e$ = concentration of dye at equilibrium (mg/L) $q_e$ = amount of dye adsorbed per amount of adsorbent at equilibrium (mg/g) $K_T$ = equilibrium binding constant (L/mg) $B_1$ = heat of adsorption

The Chi-square test statistic is basically the sum of squares of the differences between experimental data and data obtained by calculations from models with each squared difference divided by corresponding data obtained by calculation. Equivalent mathematical statement is [45]:

$$X^2 = \sum_{i=1}^m \frac{(q_{e,\text{exp}} - q_{e,\text{calc}})^2}{q_{e,\text{exp}}} \quad (5)$$

where  $q_{e,\text{exp}}$  is experimental data for equilibrium capacity (mg/g) and  $q_{e,\text{calc}}$  is equilibrium capacity obtained by calculation from the model (mg/g). If data from the model are similar to experimental data,  $X^2$  will be a

small number and if they are different  $X^2$  will be a large number [45].

For calculation of isotherms models, the SOLVER add-in in Microsoft Excel was used. Three isotherms models fitted to  $q_e$  vs.  $C_e$  graphs using nonlinear regression are displayed in Figure 8. Additionally, calculated isotherms constants, correlation coefficients ( $R^2$ ) and Chi-square test results are presented in Table 5. Results from indicate the Temkin adsorption isotherm was the best model for dye adsorption on PPSA.

### Adsorption Kinetics

Numerous kinetic models have been proposed to

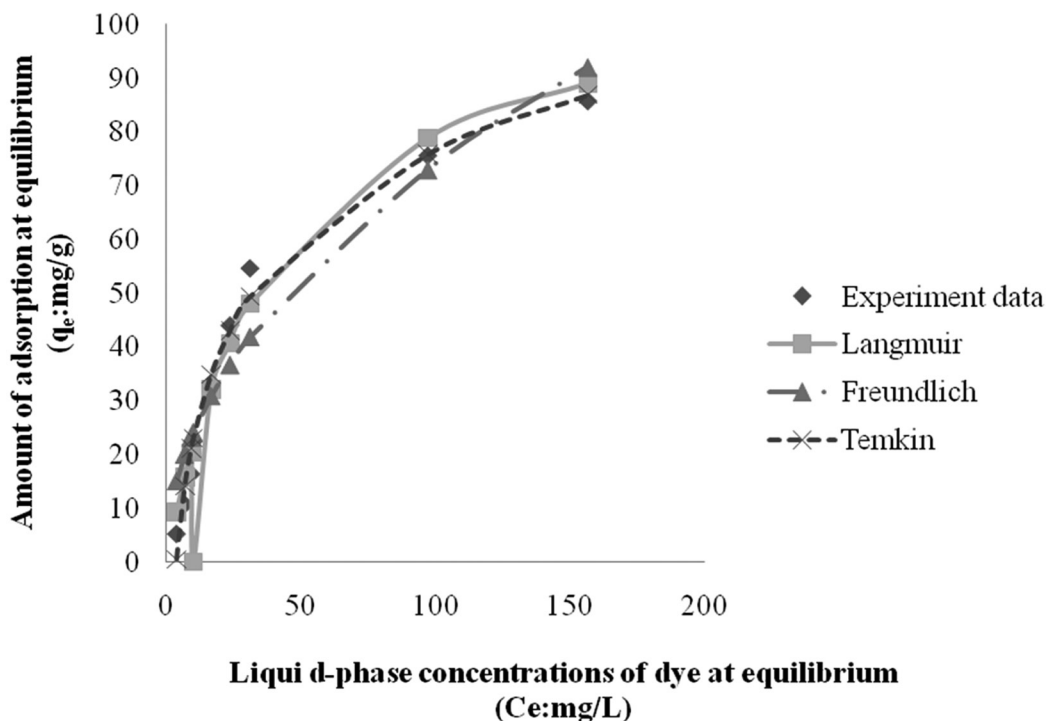


Figure 8. Adsorption isotherms of RB19 onto PPSA.

**Table 5. Adsorption Isotherms Constants.**

Isotherm Type	Isotherm Constants	R <sup>2</sup>	X <sup>2</sup>
Langmuir	$K_L = 0.0238(\text{L/mg})$ , $Q_m = 112.8646 (\text{mg/g})$	0.9788	6.88
Freundlich	$K_F = 7.8173 (\text{mg/g (L/mg)}^{1/n})$ , $n = 2.0498$	0.9761	32.22
Temkin	$K_T = 0.2695 (\text{L/mg})$ , $B_1 = 23.2079$	0.9957	7.32

elucidate the mechanism by which pollutants may be adsorbed. The mechanism of adsorption depends on physical and/or chemical characteristics of an adsorbent and on the mass transport process [48]. The kinetics parameters for the adsorption process were studied for contact time ranging from 1 to 90 minutes by monitoring the dye percent removal to investigate the mechanism of sorption. The following important kinetics models were applied in this study:

#### Pseudo-first Order Model

The pseudo-first order equation of Lagergren is expressed as follows [45]:

$$\log(q_e - q_t) = \log(q_e) - \frac{K_1}{2.303} t \quad (6)$$

where  $q_e$  and  $q_t$  are the sorption capacities at equilibrium and at time  $t$  (min), respectively (mg/g).  $K_1$  ( $\text{min}^{-1}$ ) is the rate constant. When adsorption is preceded by diffusion through a boundary the kinetics in most systems follows a pseudo-first-order equation [49].

#### Pseudo-second Order Model

The pseudo-second order model is presented by the following equation [45]:

$$\frac{t}{q_t} = \frac{1}{K_2 q_e^2} + \frac{1}{q_e} t \quad (7)$$

$K_2$  is the rate constant for pseudo-second order sorption ( $\text{g/mg.min}$ ). The pseudo-second order model is based on the assumption that the rate-limiting step may be chemical sorption involving valence forces through sharing or exchange of electrons between the adsorbent and adsorbate.

Sorption capacity is assumed to be proportional to numbers of active sites occupied on the adsorbent [20].

#### Elovich Model

The simple Elovich model equation is expressed by the following equation [45]:

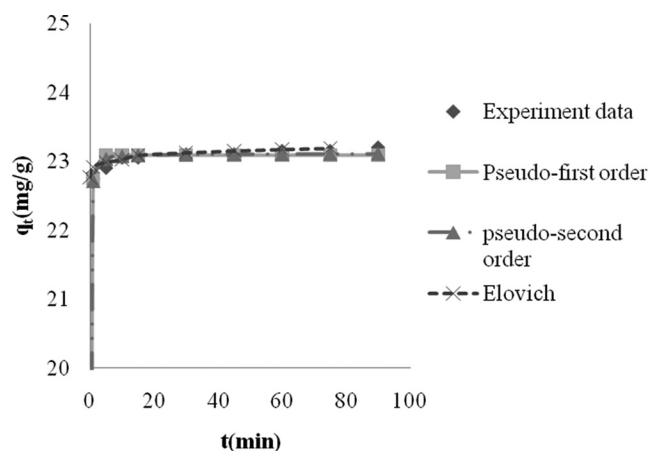
$$q_t = a + b \ln t \quad (8)$$

The slope and intercept of plot of  $q$  vs.  $\ln(t)$  were used to calculate values for the constants  $a$  and  $b$ .

SOLVER add-in in Microsoft Excel was used to calculate kinetics models. Displayed in Figure 9 three kinetics models fitted to  $q_t$  vs.  $t$  graphs by nonlinear regression. Kinetics constants and correlation coefficients ( $R^2$ ) are presented in Table 6. Results indicate that the adsorption process follows an Elovich model with an  $R^2$  of 0.999998. It is noteworthy that different of correlation coefficient of three kinetics models are very slight.

#### Treatment of Real Textile Wastewater Using PPSA

Experimentation using real textile wastewater containing RB19 dye was also done under optimal experimental conditions except for initial dye concentration. Experimental condition values of contact time were

**Figure 9.** Adsorption kinetics of RB19 onto PPSA.**Table 6. Adsorption Kinetics Constants.**

Kinetics Type	Kinetics Constants	R <sup>2</sup>
Pseudo-first order	$K_1 = -4.2236 (\text{min}^{-1})$	0.999988
Pseudo-second order	$K_2 = 2.4676 (\text{g/mg.min})$	0.999993
Elovich model	$a = 22.7685$ , $b = 0.0939$	0.999998

set at 30 min, initial pH at 11, and adsorbent dose at 4 g/L. Initial dye concentration for real textile wastewater was 500 mg/L. The dye removal efficiency and  $Q$  were obtained 59.16% and 73.86 mg/g using PPSA, respectively. However, under similar conditions (as above mentioned) for synthetic wastewater the dye removal efficiency and  $Q$  were obtained 68.65% and 85.81 mg/g, respectively.

## CONCLUSIONS

Pulp and paper industry activities are of great environmental importance due to quantities of different residuals especially sludge generated either in raw or ash forms. This work introduced pulp and paper sludge ash, a new low-cost waste material, as an adsorbent for dye removal from wastewater. PPSA appeared to be an adsorbent with a high specific surface area and its pores of different sizes and shapes was suitable for removing high concentrations of RB19. Results suggested rapid adsorption was observed in the first minutes and then became constant. Minimum and maximum removal efficiency was obtained at 29.68% and 95% and for pH at 7 and 12, respectively. Removal efficiency increased with a higher dose of adsorbent and maximum dye removal efficiency (92.59%) was observed in the highest applied adsorbent dose (12 g/L). First, with increases of initial dye concentration removal efficiency increased from 84.84% to 90% with increases of initial dye concentration ranging from 25 mg/L to 100 mg/L and then it declined from 90% to 68.65% within the range of higher initial dye concentration (100 to 500 mg/L). However,  $Q$  increased with increases of dye concentration and reached to 85.81 mg removed dye/g PPSA. The adsorption process follows a Temkin isotherm model and a Elovich kinetic model. Regarding the real textile wastewater containing RB 19, the dye removal efficiency was obtained at 59.16% using PPSA. Therefore, PPSA can be considered as a novel, natural, local, and inexpensive adsorbent for removing RB19 dye in synthetic and real textile wastewaters. Further studies may examine different factors for wide application of this adsorbent.

## ACKNOWLEDGMENT

Authors are grateful to the Amirkabir University of Technology for financial support. Authors also wish to express thanks to Ms. Lida Ezzedinloo in the Laboratory of Environmental Engineering, Department of Civil and Environmental Engineering, Amirkabir Univer-

sity of Technology, Tehran, for her assistance during experiments. In addition, we would like to gratefully acknowledge the staff of Mazandaran wood and paper industries especially Dr. Ghasem Asadpur who provided much helpful cooperation. Finally, the authors are grateful to the staff of the Alvan Sabet company for providing dye and the Negin-Nakhe-Beshel company for providing real textile wastewater.

## LIST OF SYMBOLS

ATPPS	acid treated pulp and paper sludge
BET	Brunauer–Emmett–Teller
BJH	Barrett Joyner Halenda
BTPPS	basic treated pulp and paper sludge
LOI	loss on ignition
MW	molecular weight
MWPI	Mazandaran wood and paper industries
NTU	nephelometric turbidity unit
PPSA	pulp and paper sludge ash
RB19	reactive blue 19
SEM	scanning electron microscope
XRF	X-ray fluorescence spectrometry
WW	wood waste
ZTPPS	ZnCl <sub>2</sub> treated pulp and paper sludge

## REFERENCES

1. Ofomaja, A.E., Ho, Y. S., "Equilibrium sorption of anionic dye from aqueous solution by palm kernel fibre as sorbent", *Dyes and Pigments*, Vol. 74, 2007, pp. 60–66.
2. Crini, G., "Non-conventional low-cost adsorbents for dye removal: A review", *Bioresource Technology*, Vol. 97, 2006, pp. 1061–1085.
3. Chatterjee, S., Lim, S.R., Woo, S.H. "Removal of Reactive Black 5 by zero-valent iron modified with various surfactants", *Chemical Engineering J.*, Vol. 160, 2010, pp. 27–32.
4. Bhatnagar, A., Sillanpää, M., "Utilization of agro-industrial and municipal waste materials as potential adsorbents for water treatment: A review", *Chemical Engineering J.*, Vol. 157, 2010, pp. 277–296.
5. Dawood, S., Kanti Sen, T., "Removal of anionic dye Congo red from aqueous solution by raw pine and acid-treated pine cone powder as adsorbent: Equilibrium, thermodynamic, kinetics, mechanism and process design", *Water Research*, Vol. 46, 2012, pp. 1933–1946.
6. Mittal, A., Jain, R., Mittal, J., Shrivastava, M., "Adsorptive removal of hazardous dye quinoline yellow from wastewater using coconut-husk as potential adsorbent", *Fresenius Environmental Bulletin*, Vol. 19, 2010, pp. 1171–1179.
7. Montagnaro, F., Santoro, L., "Reuse of coal combustion ashes as dyes and heavy metal adsorbents: Effect of sieving and demineralization on waste properties and adsorption capacity", *Chemical Engineering J.*, Vol. 150, 2009, pp. 174–180.
8. Zhang, W., Yan, H., Li, H., Jiang, Z., Dong, L., Kan, X., Yang, H., Li, A., Cheng, R., "Removal of dyes from aqueous solutions by straw based adsorbents: Batch and column studies", *Chemical Engineering J.*, Vol. 168, 2011, pp. 1120–1127.
9. Netpradit, S., Thiravetyan, P., Nakbanpote, W., Rattanajhonsakul, K., Tantarawong, S., Jantarangsi, P., "Waste metal hydroxide sludge as a new adsorbent", *Environmental Engineering Science*, Vol. 21, 2004, pp. 575–582.



10. Sadri Moghaddamal, S., Alavi Moghadam, M.R., Arami, M., "A comparative study of Acid Red 119 dye adsorption onto dried sewage sludge and sewage sludge ash: Isotherm, kinetic and desorption study", *J. of Residuals Science and Technology*, Vol. 7, 2010, pp. 199–207.
11. Hojamberdiev, M., Kameshima, Y., Nakajima, A., Okada, K., Kadirova, Z., "Preparation and sorption properties of materials from paper sludge", *J. of Hazardous Materials*, Vol. 151, 2008, pp. 710–719.
12. Azizi, A., Alavi Moghaddam, M.R., Arami, M., "Wood waste from mazandaran wood and the paper industry as a low cost adsorbent for removal of a reactive dye", *J. of Residuals Science and Technology*, Vol. 8, 2011, pp. 21–28.
13. Azizi, A., Alavi Moghaddam, M.R., Arami, M., "Performance of pulp and paper sludge for reactive blue 19 dye removal from aqueous solutions: isotherm and kinetic study", *J. of Residuals Science and Technology*, Vol. 7, 2010, pp. 173–179.
14. Azizi, A., Alavi Moghaddam, M.R., Arami, M., "Comparison of three treated pulp and paper sludges as adsorbents for rb19 dye removal", *J. of Residuals Science and Technology*, Vol. 8, 2011, pp. 117–124.
15. Azizi, A., Alavi Moghaddam, M.R., Arami, M., "Application of response surface methodology for optimization of reactive blue 19 dye removal from aqueous solutions using pulp and paper sludge", *Fresenius Environmental Bulletin*, Vol. 20, 2011, pp. 929–938.
16. Azizi, A., Alavi Moghaddam, M.R., Arami, M., "Application of wood waste for removal of reactive blue 19 from aqueous solutions: optimization through response surface methodology", *Environmental Engineering and Management J.*, Vol. 11, 2012, pp. 795–804.
17. Ahmad, R., Kumar, R., "Adsorption studies of hazardous malachite green onto treated ginger waste", *J. of Environmental Management*, Vol. 91, 2010, pp. 1032–1038.
18. Ip, A.W.M., Barford, J.P., McKay, G., "A comparative study on the kinetics and mechanisms of removal of Reactive Black 5 by adsorption onto activated carbons and bone char", *Chemical Engineering J.*, vol. 157, 2010, pp. 434–442.
19. Moussavi, G., Khosravi, R., "The removal of cationic dyes from aqueous solutions by adsorption onto pistachio hull waste", *Chemical Engineering Research and Design*, Vol. 89, 2011, pp. 2182–2189.
20. Ahmad, F., Daud, W.M.A.W., Ahmad, M.A., Radzi, R., "Cocoa (Theobroma cacao) shell-based activated carbon by CO<sub>2</sub> activation in removing of Cationic dye from aqueous solution: Kinetics and equilibrium studies", *Chemical Engineering Research and Design*, 2012, doi:10.1016/j.cherd.2012.01.017.
21. Gad, H. M. H., El-Sayed, A. A., "Activated carbon from agricultural by-products for the removal of Rhodamine-B from aqueous solution", *J. of Hazardous Materials*, Vol. 168, 2009, pp. 1070–1081.
22. Shi, Q., Zhang, J., Zhang, C., Nie, W., Zhang, B., Zhang, H., "Adsorption of Basic Violet 14 in aqueous solutions using KMnO<sub>4</sub>-modified activated carbon", *J. of Colloid and Interface Science*, Vol. 343, 2010, pp. 188–193.
23. Khaled, A., Nembr, A. E., Sikaily, A. E., Abdelwahab, O., "Removal of Direct N Blue-106 from artificial textile dye effluent using activated carbon from orange peel: Adsorption isotherm and kinetic studies", *J. of Hazardous Materials*, Vol. 165, 2009, pp. 100–110.
24. Demirbas, A., "Agricultural based activated carbons for the removal of dyes from aqueous solutions: A review", *J. of Hazardous Materials*, Vol. 167, 2009, pp. 1–9.
25. Haika, Y., Qadria, S., Ganoea, A., Ashraf, S., Sawafta, R., "Phase change material for efficient removal of crystal violet dye", *J. of Hazardous Materials*, Vol. 176, 2010, pp. 1110–1112.
26. Mittal, A., Kaur, D., Malviya, A., Mittal, J., Gupta, V. K., "Adsorption studies on the removal of coloring agent phenol red from wastewater using waste materials as adsorbents", *J. of Colloid and Interface Science*, Vol. 337, 2009, pp. 345–354.
27. Vimonses, V., Jin, B., Chow, C.W.K., "Insight into removal kinetic and mechanisms of anionic dye by calcined clay materials and lime", *J. of Hazardous Materials*, Vol. 177, 2010, pp. 420–427.
28. Afkhami, A., Moosavi, R., "Adsorptive removal of Congo red, a carcinogenic textile dye, from aqueous solutions by maghemite nanoparticles", *J. of Hazardous Materials*, Vol. 174, 2010, pp. 398–403.
29. Gök, O., Özcan, A. S., Özcan, A., "Adsorption behavior of a textile dye of Reactive Blue 19 from aqueous solutions onto modified bentonite", *Applied Surface Science*, 2010, Vol. 256, pp. 5439–5443.
30. Mahmoud, A.S., Ghaly, A.E., Brooks, S.L., "Influence of temperature and pH on the stability and colorimetric measurement of textile dyes", *American J. of Biotechnology and Biochemistry*, Vol. 3, 2007, pp. 33–41.
31. Konaganti, V. K., Kota, R., Patil, S., Madras, G., "Adsorption of anionic dyes on chitosan grafted poly(alkyl methacrylate)s", *Chemical Engineering J.*, Vol. 158, 2010, pp. 393–401.
32. Gong, R., Jin, Y., Sun, J., Zhong, K., "Preparation and utilization of rice straw bearing carboxyl groups for removal of basic dyes from aqueous solution", *Dyes and Pigments*, Vol. 76, 2008, pp. 519–524.
33. Vijayakumar, G., Dharmendirakumar, M., Renganathan, S., Sivanesan, S., Baskar, G., Elango, K.P., "Removal of congo red from aqueous solutions by perlite", *Clean: Soil, Air, Water*, Vol. 37, 2009, pp. 355–364.
34. Jaikumar, V., Ramamurthi, V., "Biosorption of Acid Yellow by spent Brewery Grains in a Batch System: Equilibrium and Kinetic Modeling", *International J. of Biology*, 2009, Vol. 1, pp. 21–29.
35. Kaušp?diene, D., Kazlauskienė, E., Gefeniene, A., Binkiene, R., "Comparison of the efficiency of activated carbon and neutral polymeric adsorbent in removal of chromium complex dye from aqueous solutions", *J. of Hazardous Materials*, Vol. 179, 2010, pp. 933–939.
36. Palanisamy, P.N., Sivakumar, P., "Kinetic and isotherm studies of the adsorption of Acid Blue 92 using a low-cost non-conventional activated carbon", *Desalination*, Vol. 249, 2009, pp. 388–397.
37. Tunc, O., Tanaci, H., Aksu Z., "Potential use of cotton plant wastes for the removal of Remazol Black B reactive dye", *J. of Hazardous Materials*, Vol. 163, 2009, pp. 187–198.
38. Thinakaran, N., Baskaralingam, P., Thiruvengada Ravi, K., Panneerselvam, V., Sivanesan, P. S., "Adsorptive removal of acid blue 15: equilibrium and kinetic study", *Clean: Soil, Air, Water*, Vol. 36, 2008, pp. 798–804.
39. Suteu, D., Malutan, T., Bilba, D., "Removal of reactive dye Brilliant Red HE-3B from aqueous solutions by industrial lignin: Equilibrium and kinetics modeling", *Desalination*, Vol. 255, 2010, pp. 84–90.
40. Parab, H., Sudersanan, M., Shenoy, Pathare, N.T., Vaze, B., "Use of agro-industrial wastes for removal of basic dyes from aqueous solutions", *Clean: Soil, Air, Water*, Vol. 37, 2009, pp. 963–969.
41. Ofomaja, A.E., Ho, Y. S., "Effect of temperatures and pH on methyl violet biosorption by *Mansonia* wood sawdust", *Bioresource Technology*, Vol. 99, 2008, pp. 5411–5417.
42. Asadullah, M., Asaduzzaman, M., Kabir, M.S., Mostofa, M.G., Miyazawa, T., "Chemical and structural evaluation of activated carbon prepared from jute sticks for Brilliant Green dye removal from aqueous solution", *J. of Hazardous Materials*, Vol. 174, 2010, pp. 437–443.
43. Qi Y., Hoadley, A.F.A., Chaffee, A. L., Garnier, G., "Characterisation of lignite as an industrial adsorbent", *Fuel*, Vol. 90, 2011, pp. 1567–1574.
44. Safarik, I., and Safarikova, M. "Magnetic fluid modified peanut husks as an adsorbent for organic dyes removal", *Physics Procedia*, Vol. 9, 2010, pp. 274–278.
45. Amin, N. K., "Removal of direct blue-106 dye from aqueous solution using new activated carbons developed from pomegranate peel: Adsorption equilibrium and kinetics", *J. of Hazardous Materials*, Vol. 165, 2009, pp. 52–62.
46. El Ashtouky, E.S.Z., "Loofa egyptiaca as a novel adsorbent for removal of direct blue dye from aqueous solution", *J. of Environmental Management*, Vol. 90, 2009, pp. 2755–2761.
47. Mane, V.S.I., Mall, D., Srivastava, V.C., "Use of bagasse fly ash as an adsorbent for the removal of brilliant green dye from aqueous solution", *Dyes and Pigments*, Vol. 73, 2007, pp. 269–278.
48. Zhong, Z.Y., Yang, Q., Li, X.M., Luo, K., Liu, Y., Zeng, G.M., "Preparation of peanut hull-based activated carbon by microwave-induced phosphoric acid activation and its application in Remazol Brilliant Blue R adsorption", *Industrial Crops and Products*, Vol. 37, 2012, pp. 178–185.
49. Foo, K.Y., Hameed, B.H., "Adsorption characteristics of industrial solid waste derived activated carbon prepared by microwave heating for methylene blue", *Fuel Processing Technology*, Vol. 99, 2012, pp. 103–109.

## GUIDE TO AUTHORS

1. Manuscripts shall be sent electronically to the Editor-in-Chief, Dr. P. Brent Duncan at pduncan@unt.edu using Microsoft Word in an IBM/PC format. If electronic submission is not possible, three paper copies of double-spaced manuscripts may be sent to Dr. P. Brent Duncan, (Editor of the *Journal of Residuals Science & Technology*, University of North Texas, Biology Building, Rm 210, 1510 Chestnut St., Denton, TX 76203-5017) (Tel: 940-565-4350). Manuscripts should normally be limited to the space equivalent of 6,000 words. The editor may waive this requirement in special occasions. As a guideline, each page of a double-spaced manuscript contains about 300 words. Include on the title page the names, affiliations, and addresses of all the authors, and identify one author as the corresponding author. Because communication between the editor and the authors will be electronic, the email address of the corresponding author is required. Papers under review, accepted for publication, or published elsewhere in journals are normally not accepted for publication in the *Journal of Residuals Science & Technology*. Papers published as proceedings of conferences are welcomed.
2. Article titles should be brief, followed by the author's name(s), affiliation, address, country, and postal code (zip) of author(s). Indicate to whom correspondence and proofs should be sent, including telephone and fax numbers and e-mail address.
3. Include a 100-word or less abstract and at least six keywords.
4. If electronic art files are not supplied, submit three copies of camera-ready drawings and glossy photographs. Drawings should be uniformly sized, if possible, planned for 50% reduction. Art that is sent electronically should be saved in either a .tif or .JPEG files for superior reproduction. All illustrations of any kind must be numbered and mentioned in the text. Captions for illustrations should all be typed on a separate sheet(s) and should be understandable without reference to the text.
5. DEStech uses a numbered reference system consisting of two elements: a numbered list of all references and (in the text itself) numbers in brackets that correspond to the list. At the end of your article, please supply a numbered list of all references (books, journals, web sites etc.). References on the list should be in the form given below. In the text write the number in brackets corresponding to the reference on the list. Place the number in brackets inside the final period of the sentence cited by the reference. Here is an example [2].

*Journal:* 1. Halpin, J. C., "article title", *J. Cellular Plastics*, Vol. 3, No. 2, 1997, pp. 432–435.

*Book:* 2. Kececioglu, D. B. and F.-B. Sun. 2002. *Burn-In Testing: Its Quantification and Optimization*, Lancaster, PA: DEStech Publications, Inc.

6. Tables. Number consecutively and insert closest to where first mentioned in text or type on a numbered, separate page. Please use Arabic numerals and supply a heading. Column headings should be explanatory and carry units. (See example at right.)

Table 5. Comparison of state-of-the-art matrix resins with VPSP/BMI copolymers.

Resin System	Core Temp. (DSC peak)	Char Yield,	
		T <sub>E</sub>	%
Epoxy (MY720)	235	250	30
Bismaleimide (H795)	282	>400	48
VPSP/Bismaleimide copolymer			
C379: H795 = 1.9	245	>400	50
C379: H795 = 1.4	285	>400	53

7. Units & Abbreviations. Metric units are preferred. English units or other equivalents should appear in parentheses if necessary.
8. Symbols. A list of symbols used and their meanings should be included.
9. Page proofs. Authors will receive page proofs by E-mail. Proof pages will be in a .PDF file, which can be read by Acrobat Reader. Corrections on proof pages should be limited to the correction of errors. Authors should print out pages that require corrections and mark the corrections on the printed pages. Pages with corrections should be returned by FAX (717-509-6100) or mail to the publisher (DEStech Publications, Inc., 439 North Duke Street, Lancaster, PA 17602, USA). If authors cannot handle proofs in a .PDF file format, please notify the Editor, Dr. P. Brent Duncan at pduncan@unt.edu.
10. Index terms. With proof pages authors will receive a form for listing key words that will appear in the index. Please fill out this form with index terms and return it.
11. Copyright Information. All original journal articles are copyrighted in the name of DEStech Publications, Inc. All original articles accepted for publication must be accompanied by a signed copyright transfer agreement available from the journal editor. Previously copyrighted material used in an article can be published with the *written* permission of the copyright holder (see #14 below).
12. Headings. Your article should be structured with unnumbered headings. Normally two headings are used as follows:  
Main Subhead: DESIGN OF A MICROWAVE INSTALLATION Secondary Subhead: Principle of the Design Method  
If further subordination is required, please limit to no more than one (*Third Subhead*).
13. Equations. Number equations with Arabic numbers enclosed in parentheses at the right-hand margin. Type superscripts and subscripts clearly above or below the baseline, or mark them with a caret. Be sure that all symbols, letters, and numbers are distinguishable (e.g., "oh" or zero, one or lowercase "el," "vee" or Greek nu).
14. Permissions. The author of a paper is responsible for obtaining releases for the use of copyrighted figures, tables, or excerpts longer than 200 words used in his/her paper. Copyright releases are permissions to reprint previously copyrighted material. Releases must be obtained from the copyright holder, which is usually a publisher. Forms for copyright release will be sent by the editor to authors on request.

**General:** The *Journal of Residuals Science & Technology* and DEStech Publications, Inc. are not responsible for the views expressed by individual contributors in articles published in the journal.